Influence of Molecular Order on Strong Light-Matter Interaction

Inaugural-Dissertation
zur Erlangung des Doktorgrades
der Mathematisch-Naturwissenschaftlichen Fakultät
der Universität zu Köln

Department für Chemie und Biochemie
Institut für Licht und Materialien

Vorgelegt von
Oliver Roland Schäfer
aus
Siegen

Köln
Angenommen im Jahr 2025

Abstract

In this work, we investigate the influence of molecular order on (strong) light-matter interaction. In the strong-coupling regime, the material properties are modified, e.g., chemical reactions, energy transport in transistors, and long-range energy propagation, due to newly formed hybrid states, called polaritons. We fabricate planar microcavities with the merocyanine dye HB238 that forms aggregates with both J- and H-like transitions. We achieve simultaneous strong light-matter coupling with both transitions and two different cavity modes, resulting in the formation of four polaritons. The transition dipole moment of the H-transition is perpendicular to the substrate plane, resulting in a highly polarization-dependent response of the strong-coupling behavior. This is the first report on both a strongly-coupled H-transition and a transition dipole moment located out-of-plane. We study the system with polarization- and angle-resolved reflection and emission spectra. We further fabricate microcavity samples with different numbers of coherently coupled molecules, which can be interpreted as varying dynamic disorder. We find that the H-transition requires more order than the J-transition to reach the strong coupling regime.

Next, we introduce aligned seven-atom wide armchair-edge graphene nanoribbons as a template for HB238 for light-matter studies, which yields uniaxially aligned transition dipole moments of the J-transition. In a planar microcavity we observe similar behavior as previously reported for single crystals or aligned polymers: the light-matter coupling strength is increased and the J-polaritons are highly polarization dependent due to the alignment, making templating an intriguing method to orient molecules, because it can be used for various molecules with controlled film thicknesses. We further probe the orientational order of the templated film inside the microcavity by polarization-resolved confocal microscopy and emission spectroscopy. We find that the molecules are well oriented by the seven-atom wide armchair-edge graphene nanoribbons. A multi-oscillator model is applied to both the strongly-coupled amorphous and the templated HB238 film. Mainly one polariton contributes to the coupling behavior of the templated film, indicating that the templated film consists of the aligned and a less aggregated component. The aligned component mainly contributes to the light-matter coupling.

The light-matter interaction can be tailored by other systems that confine light. We fabricate square lattices of gold nano-cylinders and deposit templated HB238 on-top to control the light-matter coupling strength by polarization. We find that the coupling strength to plasmonic lattices is largely influenced by dynamic disorder and a weaker coupling strength with templated HB238 than with amorphous layers, which contrasts the findings in planar microcavities.

Contents

1 Introduction

In the last decades, organic semiconductors have gained widespread interest for (opto-) electronic devices, both scientifically and commercially, due to the possibility to fabricate light weight, flexible devices with low cost by using scalable solution-based or evaporation methods. Both the optical and electric properties can be engineered by the choice of the molecule, making organic semiconductors highly desirable in many areas. While organic materials can be tailored for efficient conversion of light to electric energy, or vice versa, organic semiconductors often lack large charge mobility compared to inorganic semiconductors due to being limited to charge transport via the hopping process.[1–3] All of these are important properties for (opto-) electronic devices, such as organic field effect transistors[4], organic solar cells[5], or organic light emitting diodes[6]. It has been shown that the charge mobility can be improved by increasing the molecular order by fabricating single crystals[1,7,8], uniaxially aligning materials[9,10], and epitaxially growing the organic semiconductor on two-dimensional materials[11].

An emerging group of optoelectronic devices operates in the strong light-matter coupling regime. The strong-coupling regime can be reached by confining light to a small mode volume for an extended amount of time, ultimately increasing the light-matter interaction so that the interaction strength exceeds the total losses of the system.[12] The matter component in the coupled system should have a large oscillator strength, therefore e.g., J-aggregates are often used in the literature[13–15]. Under strong light-matter coupling, so-called polaritons are formed that have properties of both the light and the excitonic material. The strong light-matter regime can be reached with different geometries, e.g., planar microcavities[16], plasmonic lattices[17], photonic crystals[18], micropillars[19], and microdisks[20]. The hybrid light-matter states are discussed for several practical devices, e.g., electrically pumped polariton lasing[21], polariton organic light emitting diodes[22], quantum batteries[23], and optical transistor gates[24]. Most studies on strongly-coupled organic materials, involve disordered excitonic materials, but it has been demonstrated that the use of single crystals increases the light-matter coupling strength, which ultimately lead to the first observation of room-temperature polariton lasing[16]. Recently, Le Roux *et al.*[25] have shown that aligning a polymer increases the light-matter interaction and polarization dependence, and reduces the lasing threshold.[25] In theoretical studies it has been shown that order influences the coherence[26] and the dynamics[27,28] of the coupled system, and the strong light-matter interaction may even increase the number of coherently coupled molecules of J-aggregates[29]. Only few other examples study how the alignment[30–32] and order[33] influence the light-matter interaction.

In this dissertation we experimentally investigate the influence of molecular order on light-matter interaction and in particular on the strong-coupling regime. To answer

this scientific question, we utilize the merocyanine 2-[5-(5-dibutylamino-thiophen-2-yl-methylene)-4-*tert*-butl-5*H*-thiazol-2-ylidene]-malononitrile (HB238[34]) as model system, which allows us to influence both the dynamic and static disorder. Dynamic disorder can be influenced by annealing a thin film of HB238 at different temperatures, inducing molecular aggregation and reducing defects (increasing the delocalization of the exciton).[35,36] Dynamic disorder is a reason for broadening of the spectral features in molecular aggreates due to interactions with the molecular vibronic features. Thin films of HB238 forms molecular aggregates by oblique angle aggregation, resulting in a red-shifted (J-like) and a blue-shifted (H-like) transition. The transition dipole moments (TDMs) of J- and H-transition are perpendicular to each other: the TDM of the J-transition is located in the substrate plane, while the TDM of the H-transition is parallel to the substrate normal. With increasing annealing temperature, the J- and H-transition are shifted to lower and higher energies, respectively. Therefore, the overlap with the vibronic features of the monomer decreases with the temperature, resulting in an increased dynamic order.[36] First we incorporate thin films of HB238 that were annealed at different temperatures in planar microcavities to investigate the light-matter interaction with both the J- and H-transition. It is possible to simultaneously couple both transitions with two different cavity modes, due to a large energy difference between them. Since this is the first report of a strongly-coupled transition, with the TDM parallel to the substrate normal, we also investigate the coupling strength as a function of the location in the microcavity.

Static disorder describes for example the orientation of molecules or crystals. Orientational disorder can be probed by the polarization of light. Weitkamp[37] has demonstrated that HB238 forms uniaxially oriented crystals by using aligned seven-atom wide armchair-edge graphene nanoribbons (7-AGNRs) as a molecular template. The TDM of the J-transition is then aligned parallel to the long axis of the 7-AGNRs, while the TDM of the H-transition remains perpendicular to the substrate plane, forming a biaxial crystal.[37] We place a thin film of templated HB238 in a planar microcavity to investigate the influence of static disorder on the light-matter interaction. The system is studied in detail by polarization-resolved confocal microscopy and angle-resolved spectroscopy. We utilize the polarization splitting[38–40] of uniaxially aligned microcavities to probe the orientational order of the aggregates. We further use a multi oscillator model developed by George *et al.*[33] to investigate the influence of the dynamic disorder, which increased by the templating compared to the amorphous film.

Finally, we study the light-matter interaction of templated HB238 with plasmonic lattices. Plasmonic lattices confine light to the excitonic layer by interaction between the localized surface plasmon resonances (LSPR) in noble metal nano-particles with the diffraction order (DO) of the ordered lattice. The light component can be tailored by the shape of the nano-particles and by using different geometries of two dimensional

lattices, e.g., square, rectangular, or hexagonal[41]. In this work we use a square lattice of gold cylinders and control the light-matter interaction by the polarization-dependence of the aligned templated HB238 film.

2 Theoretical background

This chapter serves as a brief introduction to the field of light-matter interaction (Section 2.1), including both free space and systems that confine light leading to weak (Section 2.1.1) or strong (Section 2.1.2) coupling. Systems with small mode volumes required for observing strong light-matter coupling are referred to as microcavities. Section 2.2 presents the two microcavity systems utilized in this thesis: planar microcavities (Section 2.2.1) and plasmonic lattices (Section 2.2.4). Molecular aggregates were chosen as the matter component for this work, and they are discussed in Section 2.3. The molecule HB238 serves as a model system and is introduced in Section 2.3.1.

2.1 Light-matter interaction

Light-matter interaction is described by the field of quantum electrodynamics (QED). The field of QED describes the interaction or emission of electromagnetic radiation with or from charged particles (e.g. atoms or molecules). On a fundamental level, light can interact with matter by transferring the photon energy to an atom, molecule or semiconductor, which results in the promotion of an valence electron to an excited state. The excited electron can decay to the ground state by spontaneous or stimulated emission. These three fundamental light-matter interactions are sketched in Fig. 2.1 for a two-level system (ground state $|E_1\rangle$ and excited state $|E_2\rangle$). The system can decay by emission of a photon, resulting in a decay from excited to ground state of the electron. This process can either be spontaneous or triggered by another photon from an external light source. The latter case is called stimulated emission and the emitted photon has the same properties as the photon that triggered the event.[42]

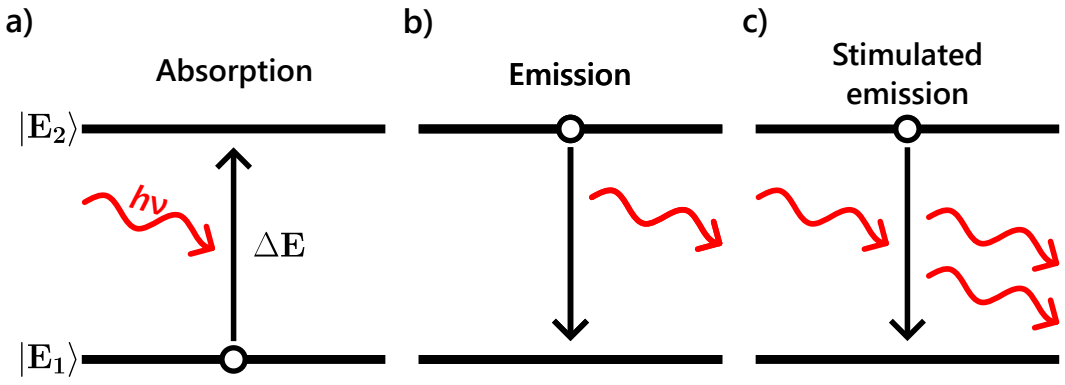

Figure 2.1: Sketch of absorption, emission and stimulated emission in a two-level system. $|E_1\rangle$ and $|E_2\rangle$ denote the ground and excited state, respectively. ΔE is the energy difference between $|E_1\rangle$ and $|E_2\rangle$. The light wave with the energy $\Delta E = h\nu$ is absorbed (a) or emitted (b, c) by the two-level system, with the Planck constant h and the frequency ν.

Practical systems interacting with light are not two-level systems. Instead, atoms,

metals, semiconductors and molecules have a more complex electronic structure, but their interaction with light can be described using two-levels in many cases. While solids are often characterized by their band structure, the different processes in molecular transitions of valence electrons after excitation can be described by the Jablonski diagram[43,44] (see Fig. 2.2). In particular, when the light-matter interaction is dominated by two energy levels, the other states can most often be ignored. This is the case for example in absorption of narrow-band light (laser light).

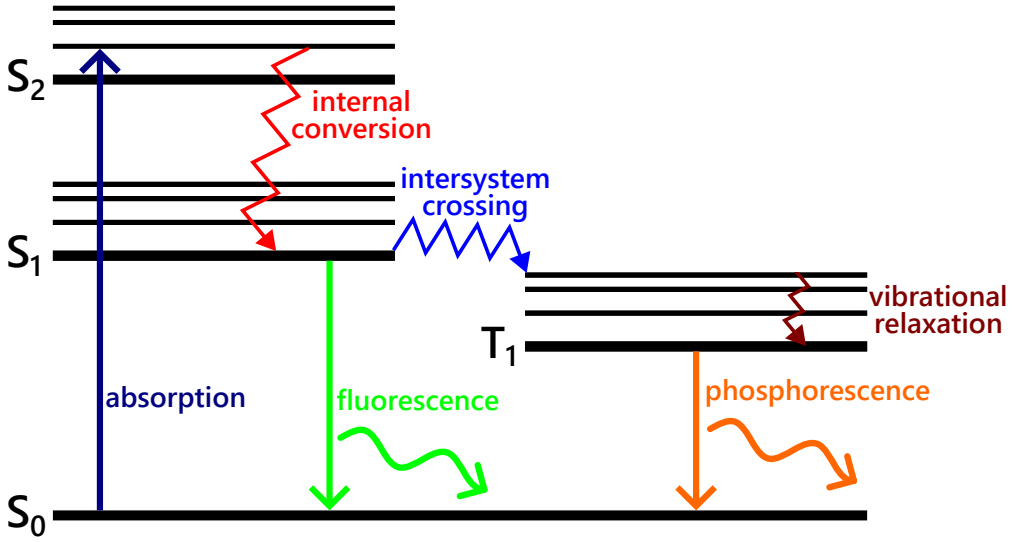

Figure 2.2: Jablonski diagram. A molecule in the ground state S_0 absorbs light to a vibrational state in the second excited singlet state S_2. The excited state decays via non-radiative internal conversion to the first excited singlet state S_1. The system can either decay to the ground state via vibrational relaxation from S_1, or decay to a triplet state (T_1). Photons can be emitted by fluorescence ($S_1 \rightarrow S_0$) or phosphorescence ($T_1 \rightarrow S_0$). Due to Kasha's rule most photons will be emitted from the first excited state.

The spontaneous decay of an excited state is exponential with a decay time of τ and can be calculated from Fermi's golden rule.[45] Here, the emission of light is treated in terms of perturbation theory as a statistic process of an ensemble of emitters. This is a quantum-mechanical treatment of the Einstein coefficients[46]. For an electric dipole with a dipole moment $\mathbf{d}$, Fermi's golden rule takes the form

$$\frac{1}{\tau} = \frac{2\pi}{\hbar^2} |\mathbf{d} \cdot \mathbf{E}(\mathbf{r},t)|^2 \rho(\omega_e), \tag{2.1}$$

with the reduced Planck constant $\hbar$, the electric field component $\mathbf{E}(\mathbf{r},t)$ of the electromagnetic field at the position of the emitter $\mathbf{r}$ at the emission frequency ω_e, and the density of the photon states the emitter with the excited state energy $\hbar\omega_e$ can radiate into $\rho(\omega_e)$. The electric field is dependent on time t and position $\mathbf{r}$.[47] Based on this golden rule, it becomes obvious that light-matter interaction is not only dependent on the matter component, but also on the density of photon states of the environment. By

placing an emitter in a system that confines light both temporally and spatially (see Section 2.2), the emission properties can be modified by the environment.[48–53]

In modifying the light-matter interaction using external structures, in microcavities, two regimes can be identified, the 'bad' and 'good' cavity domain. In the bad cavity or weak coupling regime, the photon confinement can be treated within perturbation theory and Fermi's golden rule can be applied. This results in enhancement[48] or inhibition[50] of the spontaneous emission rate.[54] In the good cavity or strong coupling regime, the system cannot be treated in terms of perturbation theory anymore. Instead, the re-absorption process of photons exceeds all losses of the coupled system and re-absorption of the emitted photon becomes a dominant process.[54] As a result, the excitation of the system is shared between the two components and it is not anymore possible to distinguish between an excited material component or cavity. The system thus has to be described in terms of new eigenstates. This will be discussed in Section 2.1.2. The energy exchange and loss processes in a planar microcavity (see Section 2.2.1) containing a two-level system is sketched in Fig. 2.3. Here, photons are reflected back and forth between two parallel mirrors (confinement of the photons). Energy is exchanged coherently between the two systems by constant absorption and re-emission by the two-level system. This light-matter interaction is described by the coupling constant g. The energy losses by the excition (e.g. non-radiative decay[55], or emission into a direction not confined by the cavity[55]) and by the cavity are denoted by γ and κ, respectively.

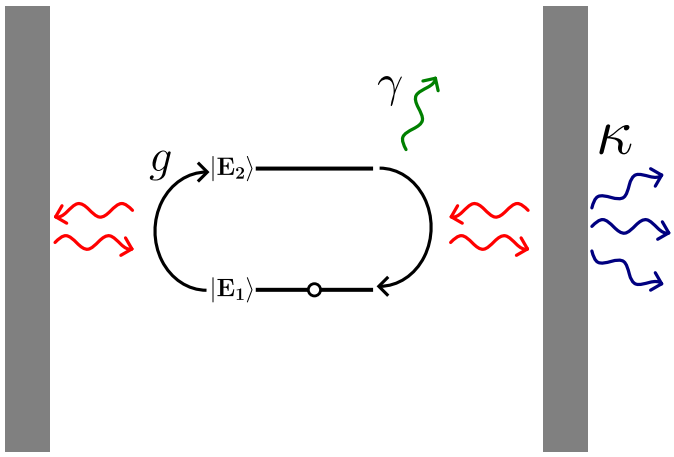

Figure 2.3: Coherent energy exchange (g) and loss mechanisms (γ, κ) between photons in a planar microcavity and a two-level system with the ground state $|E_1\rangle$ and the excited state $|E_2\rangle$.

2.1.1 Weak light-matter interaction

When a two-level system (e.g. a atom or a molecule) is placed in a confined electromagnetic field with only few modes such as a optical microcavity (see Section 2.2), the

light-matter interaction is modified and can be classified as either weak or strong. If the light-matter interaction is in the weak coupling regime, the coupling dynamics in the confined electromagnetic field can be treated as a perturbation of the spontaneous emission process. The decay of the excited state remains exponential[54] and Fermi's Golden Rule (Equation 2.1) can still be applied.[56,57] In the weak coupling regime, the total losses of the system are larger than the rate of energy exchange (coupling) between two-level system and cavity. Therefore, the probability for the emitter to re-absorb a emitted photon is smaller than the probably of the photon exiting the microcavity. The emission process can be treated as irreversible in this regime.[54]

An emitter that placed in a microcavity at a maximum of the electric field, experiences enhanced light-matter interaction, due to the spatial and temporal confinement of the photons at the position of the two-level system. A metric for the temporal and spatial confinement is the quality (Q) factor and the mode volume (V), respectively. The Q-factor is a measure for the ratio between the energy stored in the cavity and the energy loss per optical cycle and can be experimentally determined by measuring the absorbance spectra of the cavity. From the absorption spectrum the Q-factor then follows as

$$Q = \frac{\lambda}{\Delta\lambda}, \tag{2.2}$$

where λ is the resonance wavelength and $\Delta\lambda$ is the full width at half maximum of the spectral response of the cavity mode.[55] Likewise, the mode volume V is defined as the effective volume to which the mode is confined. A large Q-factor and a small mode volume lead to good confinement of photons and increased light-matter interaction. In this case the probability of a photon to interact with the two-level system is increased.

The classical model of two coupled oscillators has many parallels to light-matter interaction in microcavities: The first oscillator describes the electric field component of the photon in the cavity. The other one describes the oscillating dipole of an emitter. The two oscillators have the same oscillaton frequency. The system is damped by energy loss (κ and γ, see Fig. 2.3). Consequently, the interaction between these components can be described in the framework of two damped coupled harmonic oscillators, where the dampening describes the total loss mechanisms and the coupling strength is determined by the interaction of the oscillators (see Fig. 2.4).[58] In the weak coupling regime the effect of the presence of the second oscillator is in increasing the rate at which the other oscillator is damped, i.e., the rate at which its excited state decays. In the optical domain, this corresponds to an increased emission rate.

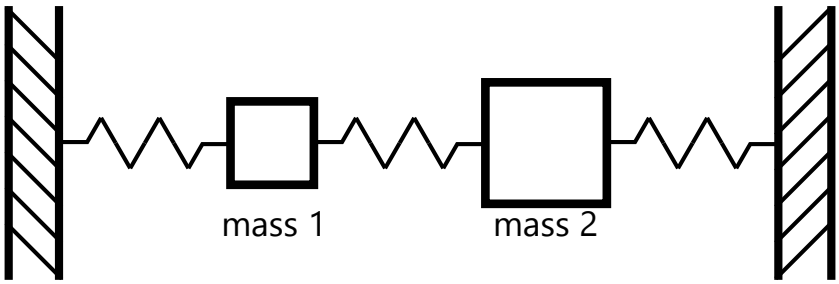

Figure 2.4: Sketch of a classical model of two coupled oscillators. Two masses are attached to walls with a spring. Another spring connects the two masses, the spring constant g defines the coupling strength of the two oscillators.

In microcavities, the photonic states become more localized and the density of photon states in the microcavity increases or decreases depending on the position within the cavity.[12] Therefore, it can be concluded from Fermi's golden rule (see Equation 2.1) that in a microcavity coupled to an emitter results in a modification of the spontaneous emission rate: If the wavelength of the cavity photon is resonant with the transition energy of the atom or molecule, the spontaneous emission rate of the transition is enhanced, if the emitter is positioned at a field-maximum. Purcell[48] first reported enhanced spontaneous emission rate in a resonator at radio frequencies. The enhancement at wavelength λ is described by the Purcell factor f

$$f = \frac{3Q\lambda^3}{4\pi^2 V}. \tag{2.3}$$

Q and V describe the quality factor (see Equation 2.2) and the mode volume of the cavity, respectively. The wavelength of the cavity photon is given by λ. This only applies for the resonant case. The Purcell factor is equal to the ratio of the spontaneous decay rate with and without the cavity structure. As can be seen from Equation 2.3, the enhancement grows with the confinement of the electromagnetic field.[48,54] If the cavity is detuned (energy of the cavity photon differs from the energy of the excited state) from the transition energy of the emitter, the spontaneous emission rate is inhibited. Kleppner[50] reported scaling of the emission rate to be proportional to $1/Q$ in this case. So in a more intuitive picture, a microcavity structure results in a highly position-dependant photon density of states.[12] This increases the probability of emission, if the cavity is resonant. In the non-resonant or detuned case, the density of states of the environment are reduced. This results in a reduction of the emission rate. To conclude, the emission rate is not a property that is only dependent on the emitter, but also on the environment.[47]

The observations of Purcell[48] and Kleppner[50] started the investigation of light-matter interaction in microcavites, which was later called cavity quantum electrodynamics (CQED). Jaynes and Cummings[59] later developed a model that describes the

interaction of one cavity mode with a two-level system and proves to be an important tool to predict vacuum Rabi oscillations, which are discussed in the next section, that become increasingly relevant in the strong coupling regime.

2.1.2 Strong light-matter interaction

In the strong coupling regime, the light-matter interaction measured with the rate of energy exchange between the two coupled components is larger than the total losses of the coupled system. In this regime, the re-absorption of emitted photons becomes the dominant process over the total losses (κ and γ). To maximize the interaction strength, the light should be confined spatially and temporally to increase the electric field, as discussed above, and by using a material component with a large transition dipole moment.[54] If the material component in the light-matter system consist of an ensemble of two-level systems, the light-matter coupling strength is proportional to the square root of the number of emitters N. With all the criteria mentioned above, the strong coupling condition takes the form[55,60–62]

$$(\kappa, \gamma) < \left(\frac{N \pi \mu^2 c}{n_{\text{cavity}}^2 \lambda_{\text{cavity}} \varepsilon_0 \hbar V} \right)^{1/2}, \tag{2.4}$$

where μ is the transition dipole moment (TDM) of the exciton, c is the speed of light, n_{cavity} is the effective refractive index of the cavity, λ_{cavity} is the resonance wavelength of the cavity, and ε_0 is the vacuum permittivity.

The strong coupling behavior in microcavities can be compared to the classical model of two coupled oscillators (see Fig. 2.4). If the oscillators have the same resonance frequency and the energy transfer between the two oscillators is large enough that it exceeds all losses, two new eigenstates arise. In this case, the oscillators will become synchronized and oscillate with a fixed phase difference. In the context of light-matter interaction in microcavities, these eigenstates are called polaritons. For the two coupled oscillators (the two-level system and the optical resonator), two polaritons are formed. The two polaritons are shifted to higher (upper polariton branch) or lower (lower polariton branch) energies compared to the energies of the uncoupled oscillators (see Fig. 2.5a). The energy difference between the two polariton states is called vacuum Rabi splitting, defined by the process of oscillating emission and re-absorption of photons by the emitter. Polaritons are quasi particles or hybrid states that have both characteristics of the involved photon and the excitonic material. Both the cavity mode and the exciton become optical dark[63] or gray[33] states, because of the strong light-matter interaction. Only the two polaritons can be optically addressed in this regime.

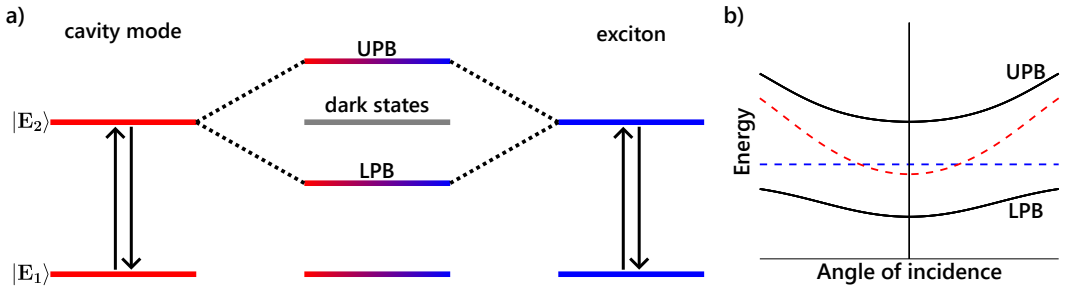

Figure 2.5: a) Formation of two hybrid states, upper (UBP) and lower (LPB) polariton branch, by strong light-matter interaction between the cavity mode (red) and the exciton (blue). $|E_1\rangle$ is the ground state of the system and $|E_2\rangle$ is the excited state of the cavity mode or the exciton. b) Angle-dependent energy diagram of polaritons (solid black lines) formed by coupling of an exciton (blue) with a planar microcavity mode (red). Dark states are indicated by a dashed line.

To investigate the strong-coupling behavior, the energy of the microcavity mode E_{cavity} is often detuned relative to the exciton energy E_{exciton}. In planar microcavities, this can be achieved by measuring reflection, transmission or emission spectra at multiple angles of incidence (AOIs), which can be done in a one-shot measurement using Fourier-transformation spectroscopy (see Section 3.1). Changing the AOI results in a change in the optical path length and increases the energy of the cavity photon with increasing AOI (see Section 2.2.1). Changing the photon energy of the cavity, results in a change of the energy of both polaritons, which are formed as a superposition of the cavity mode and the exciton of the material component. This is evidence, that both of the observed eigenstates have a character of the cavity state. This is an unambiguous proof of the formation of coupled states. If the cavity is negatively detuned ($E_{\text{cavity}} < E_{\text{exciton}}$ at 0° AOI), the lower polariton branch has more excitonic character at normal incidence and gets more photonic at large angles. This behavior reverses for the upper polariton branch. A consequence of the strong coupling is that the energy of the polaritons never becomes equal to that of the two coupled components (see Fig. 2.5b). This behavior is often called anti-crossing and it is considered a hallmark of strong light-matter interaction.

In this work, the strong-coupling behavior is analyzed with the Hopfield model.[64–66] In this model, light-matter coupling is described in terms of electromagnetic waves interacting with excitons.[12] Here, the exciton and the electromagnetic waves are treated as coupling two coupled oscillators and can be described using the following Hamiltonian model

$$\begin{pmatrix} E_{\text{cavity}} & \hbar\Omega/2 \\ \hbar\Omega/2 & E_{\text{exciton}} \end{pmatrix} \begin{pmatrix} \alpha \\ \beta \end{pmatrix} = E_{\text{polariton}} \begin{pmatrix} \alpha \\ \beta \end{pmatrix}, \tag{2.5}$$

where E_{cavity}, E_{exciton} and $E_{\text{polariton}}$ are the energy of the cavity photon, the exciton, and the polariton, respectively. The matrix on the left side is a 2x2 Hamiltonian matrix describing the interactions of the system. The eigenvector contains the Hopfield

coefficients which are related to the photon ($|\alpha|^2$) and exciton ($|\beta|^2$) fraction of the formed polariton state.[65] The interaction strength between the cavity and the exciton is quantified by the coupling constant ($\hbar\Omega/2$). Equation 2.5 can be solved to give the energies of the polaritons. Due to the 2x2 nature of the Hamiltonian, there are always two solutions. For the case of uncoupled oscillators, the energies of the polaritons are reduced to those of the oscillators, E_{cavity} and E_{exciton}. For non-zero coupling, $\hbar\Omega > 0$, the solution is[66]

$$E_{\text{polariton}} = \frac{E_{\text{cavity}} + E_{\text{exciton}}}{2} \pm \frac{1}{2}\sqrt{\left(E_{\text{cavity}} - E_{\text{exciton}}\right)^2 + (\hbar\Omega)^2}. \tag{2.6}$$

The energetic splitting of the two polaritons depends on the coupling or Rabi energy $\hbar\Omega$. Since the linewidth of the transitions is non-zero, this splitting can only be observed if the coupling is sufficiently large. We say that the system is strongly coupled, if $\hbar\Omega/2$ is larger than the spectral linewidth of both the cavity photon mode and the exciton.[55,67]

Strong light-matter interaction is an interesting research field, due to the hybrid nature of the polaritons, combining both photonic and excitonic properties. For microcavities, a multitude of different geometries can be used, as discussed in Section 2.2. Strong coupling has been demonstrated for atoms[68], inorganic semiconductors[69], quantum dots[70], and organic semiconductors[13]. Organic Frenkel excitons have larger binding energies than Wannier-Mott excitons, found in inorganic semiconductors, which results in larger coupling strengths in organic light-matter hybrid systems.[55] Under strong light-matter interaction the properties of the excitonic material are changed. It has been demonstrated that strong coupling influences chemical reactions[71,72], energy transport in transistors[73–75], long-range energy propagation[76,77] and polariton mediated energy transfer between different dyes[78,79]. Based on the unique properties in this regime, various applications have been realized or proposed, such as lasing at room temperature[80], polariton organic light emitting diodes[22], quantum batteries[23] and optical transistor gates[24]. Strong light-matter interaction gives a unique opportunity to shape the optical properties of materials by coupling them to cavity structures.[12]

2.2 Microcavities

The term microcavity describes systems that confine light to small mode volumes for an extended amount of time. A metric for the temporal confinement is the Q-factor as defined and discussed in Equation 2.2. Confining light to small mode volumes and achieve large Q-factors can be realized with a multitude of different geometries and materials. In this section, the planar optical microcavity, plasmonic structures and surface lattice resonances will be briefly introduced. These systems were used in this work to study strong light-matter interaction. In literature, light-matter interaction has also be studied with a multitude of other systems, for example micropillars[19], microdisks[20] and photonic crystals[18].

2.2.1 Planar microcavities

Planar or Fabry-Pérot microcavities are made of two parallel mirrors with an optical path length of few multiples of half a wavelength between them (see Fig. 2.6). If this resonance condition is met, a standing wave can form by interference of the reflected light wave with itself. The cavity consist of vertically stacked layers, offering a simple fabrication route: depositing a metal or Bragg mirror on a substrate, followed by a dielectric or emitter layer and a semitransparent mirror, closing the microcavity. Planar microcavitis are often studied in literature, due to the ease of fabrication, while offering low losses, especially if Bragg reflectors are used. Therefore, planar microcavities have sufficiently large Q-factors to reach the strong coupling regime with a multitude of emitters. For these reasons planar microcavities are used in the studies presented and discussed in Sections 4.1 and 4.2.

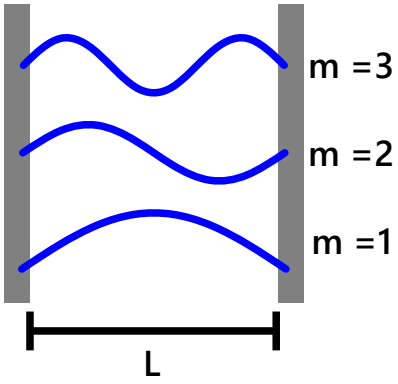

Figure 2.6: Sketch of a planar microcavity consisting of two parallel mirrors with the distance L between them. Three resonant modes ($m = 1, 2, 3$) are illustrated here.

A ideal microcavity with perfectly reflective mirrors can be compared to a quantum mechanical particle in a box. The electric field component along the mirror surface (in-plane) is zero at both mirror interfaces. Therefore, the allowed in-plane cavity modes

are sine shaped standing waves as sketched in Fig. 2.6.[54] The photon energy E_0 of the modes at 0° AOI can be calculated as:

$$E_0 = \frac{hcm}{2n_{\text{cavity}}L}, \tag{2.7}$$

where h is the Planck constant, c is the speed of light in vacuum, m is the cavity mode number that can be any natural number (see Fig. 2.6), n_{cavity} is the effective refractive index inside the cavity, and L is the physical distance between the mirrors. This Equation can be used to estimate the required distance between the mirror to tune the cavity on resonance with the photon energy of the transition in the emitter.[55]

If the AOI θ of the light is not zero, the photon energy of the allowed cavity modes increases with the angle (see Fig. 2.7). The angle-dependent photon mode of the cavity photon is given by[55]

$$E_{\text{cavity}}(\theta) = E_0 \left(1 - \frac{\sin^2\theta}{n_{cavity}^2}\right)^{-1/2}. \tag{2.8}$$

The possibility to modify the energy of the supported mode by varying the AOI, makes planar microcavities an attractive platform, because the light-matter interaction can be (de)tuned by changing the AOI. This property helps investigating the coupling behavior, because anti-crossing behavior can be probed by changing the AOI as a proof for the strong-coupling condition. Note that the angle-resolved spectra also depend on the polarization of the incident light field. The s- and p-polarized light exhibit different phase changes at both metal and Bragg mirrors at non-zero AOI, resulting in different angle-dependent spectra.[66,81]

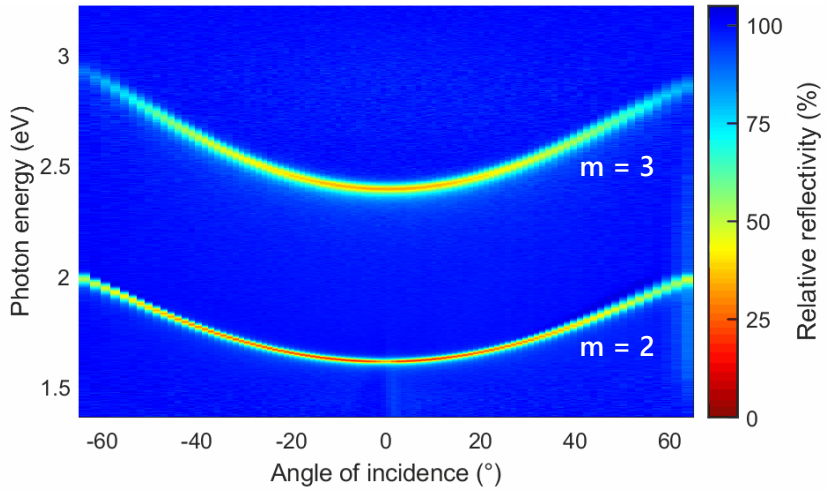

Figure 2.7: Measured angle-resolved reflectivity (see Section 3.1) of a microcavity fabricated with two parallel silver mirrors and a dielectric spacer in-between, illuminated with s-polarized light. The cavity supports the m = 2 and 3 modes in the photon energy range shown here.

If the microcavity is illuminated with p-polarized light at non-normal incidence, a out-of-plane component of the electrical field emerges. The boundary condition that the electric field is zero at the mirror interface does not apply for the out-of-plane component of the electric field. Instead, the p-polarized electric field component exhibits a phase change at the mirror interface[82], resulting in a cosine shaped standing wave as sketched in Fig. 2.8).[54] The strongest light-matter interaction occurs at the anti-nodes of the electric field components and the anti-nodes of the in- and out-of-plane electric field component occur at different positions in the cavity (see Fig. 2.8). Therefore, emitters with aligned TDMs can be selectively addressed by the respective electric field component. This allows for controlling the light-matter interaction in great detail.

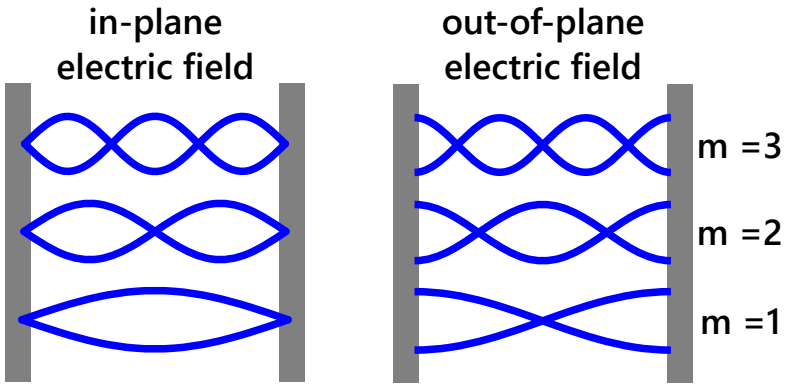

Figure 2.8: Sketch of the in- and out-of-plane modes in an optical microcavity. Standing waves form due to interference after being reflected at a mirror interface.

The ease of fabrication, the large Q/V-ratio, the angle-dependent spectral positions of the cavity modes, and the support of out-of-plane optical modes makes this a ideal platform to investigate strong light-matter interaction and was used for these reasons in the studies presented in Sections 4.1 and 4.2.

2.2.2 Plasma excitations

The field of Plasmonics describes the optical phenomenon of collective oscillations of electrons in the conduction band. The free electrons in the conduction band of metals can be treated as an electron gas cloud (plasma) that can move freely within the metal lattice as described in the Drude-Sommerfeld model.[56,83,84] After an optical excitation, the electrons oscillate with the electric field, resulting in local changes in the charge density. Based on the Drude-Sommerfeld model, the optical response of metals can be described by the complex dielectric function[56]

$$\varepsilon_{\text{Drude}} = 1 - \frac{\omega_{\text{P}}^2}{\omega^2 + \Gamma^2} + \mathrm{i}\frac{\Gamma\omega_{\text{P}}^2}{\omega\left(\omega^2\Gamma^2\right)}, \tag{2.9}$$

with the volume plasma frequency ω_P that describes the longitudinal oscillations of the plasma (also called volume plasmon)[56]:

$$\omega_P^2 = \frac{ne^2}{\varepsilon_0 m_e},$$

where n is the number of electrons per unit volume, e and m_e is the charge and mass of the conduction band electrons, respectively. In Equation 2.9, Γ is a damping factor and describes the average collision frequency of the electrons and ω is the angular frequency of the excitation light. The model accurately reproduces the optical response of metals, but is less accurate for frequency ranges, where interband transitions occur. The Drude-Sommerfeld model predicts the dielectric function well for noble metals, such as gold and silver, at optical frequencies with some limitations.[56,84]

In the high energy regime, interband transitions can be induced by optical excitation in metals. For gold, the conduction band consists of 6sp hybrid orbitals. By optical excitation, an electron can be promoted from the 5d to the 6sp orbital. This interband transition can be observed at photon energies from 2.4 eV.[84,85] In order to also take frequency independent interband transitions into account, but keep the simplicity of the Drude-Sommerfeld model, an offset ε_0 can be introduced as:[84]

$$\varepsilon_{\text{Drude,Interband}} = \varepsilon_0 - \varepsilon_{\text{Drude}}. \tag{2.10}$$

This model reproduces the real part of the dielectric function well, but fails to reproduce the imaginary part above 1.8 eV[84]. To further improve the accuracy of the dielectric function of gold, more complex models have been proposed.[84]

From equation 2.9 it can be deduced that, if $\omega < \omega_P$ the real part of $\varepsilon_{\text{Drude}}$ is smaller than zero and the imaginary part is small. If this condition is fulfilled, plasma oscillations of the free conduction band electrons are supported and can be excited by light. These plasma oscillations of conduction band electrons in metals are referred to as plasmons.[56] In the spectral regions, where plasmons are supported, interesting optical properties can be observed. The field studying and applying plasmons is known as plasmonics.[56,83,84] There are two main types of plasmon excitations that are exploited in the field in plasmonics: i) Surface plasmon polaritons, where the electron cloud is excited parallel to the metal surface at the interface between a dielectric and a metal, launching charge density oscillations along the metal-dielectric interface under certain conditions, and ii) localized surface plasmon resonances, which describes the optical response of metal particles smaller than the excitation wavelength. The electron gas in the particles oscillates with the electric field and which in turn acts as an oscillating dipole. Here the plasmon wave does not propagate, giving the name of the excitation. Both i) and ii) lead to a strong near-field enhancement (large Q/V-ratio), due to the very

small V, that can be utilized to enhance the light-matter interaction. Localized surface plasmon resonances will be briefly introduced in the following section.

2.2.3 Localized surface plasmon resonance

Localized surface plasmon resonances (LSPR) are non-propagating surface plasmon that are localized in a small volume of metal nano-particles with sizes smaller than the excitation wavelength. The excitation of the electron gas results in a strong near-field enhancement around the particle of much smaller mode volumes than in for example planar microcavities (see Chaper 2.2), resulting in a strong near-field enhancement.[86] Therefore, these nano-particles are often referred to as nano-cavities or optical antennas.[56,86–88] However, the excitations are lossy resulting in lower Q-values than for microcavities. The light-matter interaction strength is thus similar in these two systems.

If the particle is much smaller than the wavelength and is illuminated with a plane wave, the electron plasma in the particle starts oscillating, resulting in a temporal charge separation. The electrons are displaced with respect to the applied electric field (sketched in Fig. 2.9). Therefore, the particle can be approximated as a radiating dipole, with the scattered light as emission from the dipole.[87,89] The wavelength of the LSPR are dependent on the particle size, shape, dielectric environment, and particle metal. For gold nano-particles the LSPR are typically supported in the visible spectral range.[84,87,89]

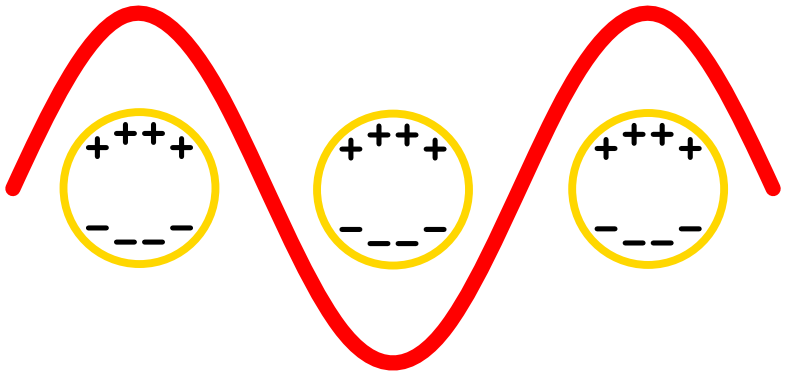

Figure 2.9: Sketch of localized surface plasmon resonances in a gold nano-particle after excitation with an electric field (red). The conduction band electrons begin to oscillate due to the applied electric field, causing charge separation at the particle surface.

While the mode volume for nano-particles is small[86], the Q-factor is not as large as for other microcavities[87]. Regardless, strong coupling has also been realized in literature[90]. To improve on this limitation, plasmonic nano-particles can be coupled to diffraction orders (DOs) of a photonic crystal by placing them in an ordered array. Consequently, the temporal confinement of light is enhanced. The collective excitation

of an plasmonic nano-particle array is called surface lattice resonances (SLR), which is discussed in the next section.

2.2.4 Surface lattice resonances

Plasmonic surface lattice resonances (SLR) are phenomena of collective coherent scattering of light at an ordered lattice of many plasmonic nano-particles. Auguié and Barnes[91] first observed sharp resonances in transmission spectra of gold nano-rod arrays. The sharp spectral features can be explained by resonant coupling of the LSPR, which can be approximated as radiating dipoles, and the diffraction orders (DOs) of the lattice. The incoming light waves are scattered between the plasmonic particles, resulting in a strongly enhanced temporal confinement. The tunable properties of plasmonic lattices are the size and shape of the particles and the period of the lattice (see Fig. 2.10a).[41,87] A transmission spectrum of a plasmonic nano-particle lattice with a sharp SLR dip is shown in Fig. 2.10b.

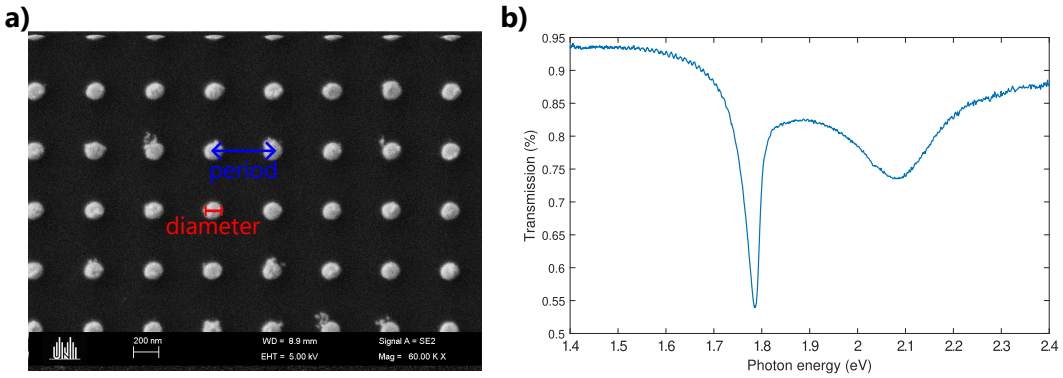

Figure 2.10: a) Scanning electron micrograph of a gold nano-disk array with a period of 475 nm. b) Transmission spectrum of a gold nano-disk lattice with a 457 nm period. The nano-particle diameter and thickness in both panels is approximately 92 nm and 50 nm, respectively. The sharp surface lattice resonances (SLR) peak is observed at approximately 1.8 eV.

For SLR to appear, the size of the nano-particle has to be tuned so that the LSPR of the particle is close to the spectral positions of the DO of the lattice. Auguié and Barnes[91] fabricated arrays with gold particles sized from 50 to 120 nm and a thickness of approximately 35 nm for the LSPR to be in the visible wavelength spectrum. The lattice constant was varied from 480 to 560 nm, ensuring that the DO is spectrally close to the LSPR. This configuration resulted in the observation of sharp extinctions with wavelengths of 700 to 800 nm, depending on the array period and the particle size.[91]

The spectral positions of the DO and therefore the approximate positions of the SLR can be calculated by using the primitive reciprocal lattice vectors. This method has been demonstrated by Guo *et al.*[41] for different lattice geometries. In the following paragraph the process will be briefly reviewed for square and rectangular lattices.

The particle array is illuminated with a plane wave and scattered at the particles. The scattered wave can also be approximated as a plane wave. The basis vectors of the reciprocal lattice are

$$\overrightarrow{b_1} = \frac{2\pi}{p_x}\begin{pmatrix}1\\0\end{pmatrix} \tag{2.11}$$

and

$$\overrightarrow{b_2} = \frac{2\pi}{p_y}\begin{pmatrix}0\\1\end{pmatrix}, \tag{2.12}$$

where p_x and p_y are the lattice period in x- and y-direction ($p_x = p_y$ for a square lattice). These are inserted into the reciprocal lattice vector is

$$\mathbf{G} = m_1\overrightarrow{b_1} + m_2\overrightarrow{b_2}, \tag{2.13}$$

where m_1 and m_2 are integers and correspond to the DO (see Fig. 2.11a). The photon energy E of the DO can then be calculated as

$$E = \frac{\hbar c}{n}|\mathbf{G} + k_y|, \tag{2.14}$$

where n is the refractive index of the medium around the array and k_y is the in-plane wave vector of the incident light in the y-direction. This equation can be intuitively understood by the sketch in Fig. 2.11a. Here, we probe the angular direction of the scattering in the y-direction. The DO $(m_1 = 0, m_2 = 1)$ and (0,-1) scale linearly with increasing k_y and split into two branches, while the DO (1,0) and (-1,0) have a non-linear dependence of k_y. Note that the (1,0) and (-1,0) modes are accessible with p-polarized light and the (0,1) and (0,-1) can be excited with s-polarized light.[41]

One way to characterize SLR is by varying the AOI θ, because the in-plane wave vector is dependent on the wavelength λ and angle θ as

$$k_y = \frac{2\pi}{\lambda}\sin\theta. \tag{2.15}$$

The calculated DO are plotted in Fig. 2.11b. Alternatively, the reciprocal space can be analyzed by measuring many arrays with different grating periods at normal incidence. This also detunes the spectral position of the SLR (see Fig. 2.11c). In this case, the reciprocal lattice spacing k is plotted, which is given by[17]

$$\mathrm{k} = \frac{2\pi}{h}. \tag{2.16}$$

The spectral dependence lattices as a function of the AOI or the lattice spacing can be studied in transmission or reflection experiments.

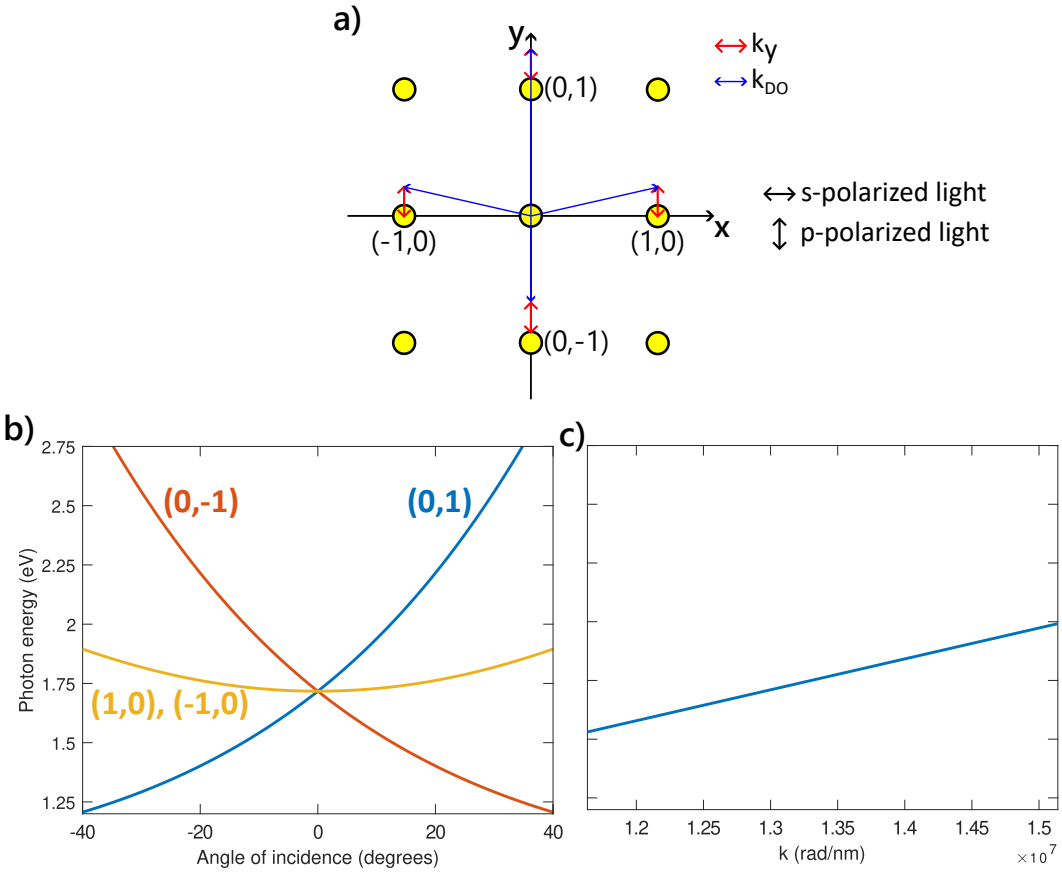

Figure 2.11: a) Interaction of the in-plane wave vector k_y with a lattice. Here sketched is the reciprocal space, indicating the scaling of the diffraction order by increasing k_y. b) Calculated diffraction order for a square lattice with 475 nm period in a medium of refractive index 1.52. c) Calculated spectral position of diffraction order as a function of the reciprocal lattice spacing for a square lattice in a medium of refractive index 1.5 with a lattice period from 415 nm to 540 nm. The diffraction orders are degenerate at normal incidence. Plotted is the reciprocal lattice spacing $\mathrm{k} = 2\pi/h$, where h is the Planck constant. Concept adapted from Guo *et al.*[41].

As previously mentioned, sharp SLR are observed, when the DO is tuned spectrally close to the LSPR. Other requirements for narrow SLR are the following: i) large spacial coherence to excite the whole array. Therefore, objectives with a small numerical aperture (NA) are necessary (NA < 0.5) to investigate SLR.[87] ii) The refractive index of the environment needs to be homogeneous around the particle array. This is only a strict requirement at normal incidence. The refractive index mismatch between the substrate and the material embedding the particles can be larger at large AOIs.[87,92] iii) The particle array needs to be sufficiently large, as the Q-factor scales with lattice size.[87,93]

Lattices of plasmonic nano-particles are typically fabricated using electron-beam lithography, followed by the evaporation of a metal (commonly gold or silver). After a lift-off procedure the particles are formed on the substrate. This makes SLR relatively accessible in terms of fabrication. The angle- or period-dependent detuning of the spec-

tral position simplifies the investigation of strong light-matter interaction. This is made possible by using electron-beam lithography to create a multitude of lattice structures. As demonstrated by Väkeväinen *et al.*[17], the large Q-factor allows for enhanced light-matter interaction, ultimately reaching the strong coupling regime.

2.3 Molecular Aggregates

Organic molecules can aggregate by self-assembly, forming so called J- ("Jelley-") or H- (hypsochromic-) aggregates. Notable examples for molecules, that form aggregates, are cyanine, merocyanine, and squarine dyes.[94] Depending on the molecular stacking either J- or H-aggregates are formed. J-aggregates are characterized by a sharp absorption peak that is red- (bathochromically) shifted relative to the monomer, a remarkably small Stokes shift and an increased emission rate. Conversely, when H-aggregates are formed, the absorption band is blue- (hypsochromically) shifted and the emission of photons is inhibited.[94,95]

What later became known as J-aggregates were first observed by Jelley[96] and Scheibe[97,98], respectively. Both researchers reported that pseudoisocyanine chloride exhibits a red-shifted absorption relative to the dye in a good solvent. Furthermore, they observed an increased emission with a small Stokes shift. Scheibe correctly attributed this effect to "reversible polymer chains" of the dye molecules due to Van der Waals forces, which was later confirmed[99,100]. The TDM of the molecules is in this case arranged in a "head-to-tail" configuration, leading to the formation of J-aggregates and their distinctive optical properties.[95] Due to their unique properties, J-aggregates have attracted significant interest in various research areas such as organic field-effect transistors[101] and solar cells[34].

H-aggregates are formed by molecular stacking with the TDM aligned "side-by-side".[95] In contrast to J-aggregates, H-aggregates exhibit a blue-shifted absorption spectrum relative to the monomer and generally display non-emissive properties. However, there are exceptions where H-aggregates were red-shifted[102] and some examples show emission[103].[94,95,104]

Kasha[105,106] developed the first exciton model that could qualitatively describe the spectral behavior of H- and J-aggregates. By theoretically investigating dimers and linear chains with side-by-side, head-to-tail, and oblique angle configurations, he demonstrated how J- and H-aggregates are formed by bringing molecules to close proximity via van der Waals forces. The molecules interact through Coulomb coupling of the transition dipole moments, resulting in J- and H-transitions.[95,105,106]

When molecules are brought into close proximity through aggregation, the different environment causes a shift in the energy of their excited state. This "gas-to-crystal" energy (D) is typically negative and can result in red-shifted absorption spectra observed in some H-aggregates when the molecules exhibit weak Coulomb coupling.[102] If a dimer is formed in a side-by-side fashion, a H-transition can be observed in the absorption spectra. When the TDM (sketched as a vector in Fig. 2.12) are arranged in parallel, their vector sum results in an increased oscillator strength and is therefore optically allowed. This configuration is energetically less favorable (shifted to higher energies)

than the anti-parallel case, where the total oscillator strength vanishes and cannot be excited. The H-transition is nonemissive, because the higher energy state is optically allowed, while the lower energetic state is forbidden (Kasha rule[107]).[95,105,106]

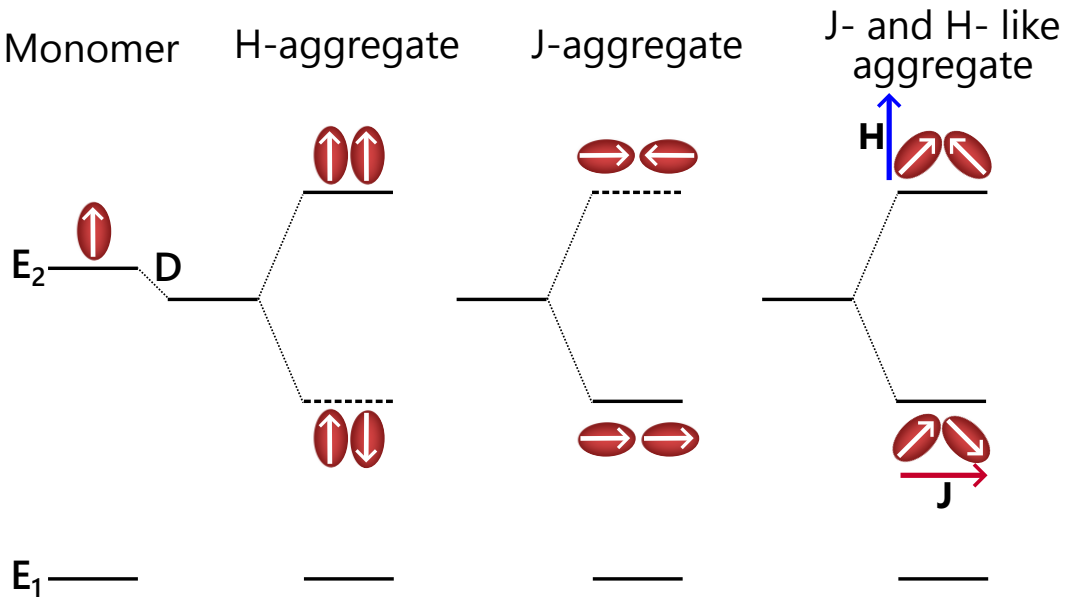

Figure 2.12: A sketch of different molecular arrangements between two monomers, forming a dimer. This dimer model can be used to illustrate the formation of either H-, J-aggregates or a mixture. E_1 and E_2 are the ground and excited state of the monomer, respectively. D is the gas-to-crystal shift. Concept adopted from Kasha[105], Hestand and Spano[95].

In the head-to-tail arrangement of the TDMs, J-aggregates are formed. The energetically favorable and optically allowed configuration occurs when both TDMs couple constructively with their vectors pointing in the same direction (Fig. 2.12). Conversely, if TDMs point towards each other, they lie at higher energies and are optically forbidden. J-aggregates can also be observed if not in ideal head-to-tail configuration. If the slip angle (defined by 0° in head-to-tail and 90° in side-by-side, see Fig. 2.13) is smaller than 54.7°, J-aggregates are formed; otherwise, H-aggregation result when the slip angle is larger than 54.7°.[95,105,106]

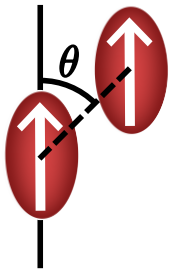

Figure 2.13: Definition of the slip angle θ. Concept adapted from Hestand and Spano[95].

The lineshape of the aggregates cannot be directly explained within the Kasha excitation model, as coupling to molecular vibrations is neglected.[95] According to Eisfeld and Briggs[104], J-transitions typically shows extraordinary narrow peaks due to being shifted to a spectral region with no monomer electronic vibration coupling. On the other hand, H-transitions have considerable overlap with molecular vibronic features, resulting in broadening of the peak in the weak and intermediate molecule-molecule coupling regime.[104]

In oblique angle aggregation of two monomers, both possible alignments of the TDMs are allowed, resulting in the observation of both J- and H-like transitions. In the graphical picture of Fig. 2.12, the vector sum and difference of TDMs result in a J-like and H-like transition, respectively.[95,105] Both addition and subtraction yield increased oscillator strength and result in two allowed states that share the same ground state. Both states can be optically excited; however, only the J-transition is emissive due to Kasha's rule. This has been experimentally demonstrated with 3,3-bis(sulfopropyl)-5,5-dichloro-9-ethylthiacarbocyanine (THIATS)[108] and 2-[5-(5-dibutylamino-thiophen-2-yl-methylene)-4-*tert*-butyl-5*H*-thiazol-2-ylidene]-malononitrile (HB238)[36].

The oblique angle case can also be explained within the framework of Davydov splitting[109,110]. In this theory, molecular crystals with two or more translationally non-equivalent molecules within a primitive unit cell are expected to have a red-shifted and blue-shifted absorption peak (in this work called H- and J-like transitions). One of Davydov's results is that the H- and J-like transitions are oriented perpendicular to each other,[109,110] which leads to a strongly polarization-dependent response. This type of aggregate is investigated in this work, and the utilized dye is detailed in the next Section 2.3.1.

Aggregates typically do not consist of simple dimers; instead, they are built from molecular chains. As mentioned earlier, it was found that pseudoisocyanine chloride forms worm-like aggregates with a few hundred nanometers in length.[99,100] Despite the size of the aggregate, the exciton is not delocalized over all molecules in the chain, due to defects. The number of coherently coupled molecules serves as a metric for the exciton coherence length and describes how many molecules the excitation is delocalized over. This number significantly influences the optical properties of the aggregate.[95] The number of coherently coupled molecules can be determined using various spectroscopic methods, as detailed by Jumbo-Nogales *et al.*[111].

2.3.1 The merocyanine dye HB238

The molecule 2-[5-(5-dibutylamino-thiophen-2-yl-methylene)-4-*tert*-butl-5*H*-thiazol-2-ylidene]-malononitrile (shown in Fig. 2.14a) belongs to the group of merocyanines and serves as a model system for this work and the optical properties will be discussed in

this Section. From now on, this dye will be referred to as HB238, following the first publication by Bürckstümmer[34].

As the name implies, merocyanines are similar to cyanine dyes but are charge neutral (non-ionic). Merocyanines consist of an electron donor and an electron acceptor with a polymethine group in between. The polymethine chain forms a conjugated system where the π-electrons are delocalized, making them ideal dye molecules due to their ability to absorb visible to infrared light, depending on the specific chemical structure.[34,94]

The consequences of the aggregation of HB238 is depicted in Fig. 2.14b-d. The transmission spectrum of unaggregated HB238 (obtained by incorporating it into a polymer matrix) is shown in Fig. 2.14b. It exhibits an absorption maximum at approximately 1.9 eV and displays vibronic features. Upon aggregation in a spin-cast and annealed thin film, the vibronic features disappear, leaving only a sharp, red-shifted peak (1.65 eV) visible in the transmission spectrum at normal incidence (see Fig. 2.14c and d). When the sample is illuminated with p-polarized light at a non-zero AOI, a second blue-shifted peak (2.53 eV) emerges (see Fig. 2.14d). This peak cannot be observed using s-polarized light at any AOI (see Fig. 2.14c). From this data, it can be concluded that HB238 aggregates in an oblique angle fashion, resulting in both a J- and H-like transition. The highly polarization and angle-dependent response can be interpreted as follows: the TDM of the J-transition is located in the substrate plane, while the TDM of the H -transition is parallel to the substrate normal. Calculations using density function theory have confirmed this and shown that in a crystal of HB238, the J-transition is parallel to one crystallographic axis, while the H-transition is perpendicular to this. Therefore, HB238 forms biaxial single crystals.[35,36,112]

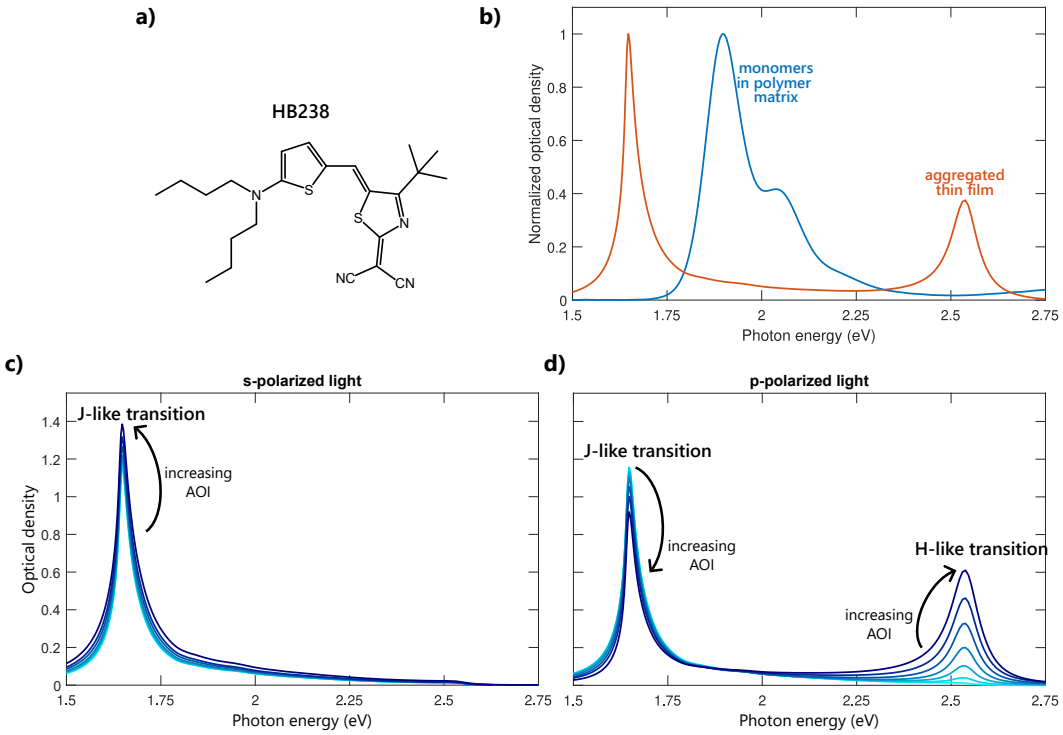

Figure 2.14: a) Chemical structure of HB238. b) Comparison between transmission spectra of unaggregated monomers in a polymer matrix at normal incidence and a thin film of HB238 at an angle of incidence of 45°. c) and d) show transmission spectra of an aggregated thin film of HB238 for s- and p-polarized light, respectively.

It has been shown that the molecular order of the HB238 aggregates can be controlled by the annealing temperature. The molecule-molecule coupling starts in the weak (minor traces of aggregation in the spectrum), transitions to the intermediate (overlap of the H-transition with the molecular vibronic progressions) and finally enters the strong coupling regime (both transitions are spectrally sharp).[35,36,112] Böhner *et al.*[35,36] have shown that this can be attributed to an increase in the number of coherently coupled molecules, which indicates an increase in order. An in-depth investigation on the optical and electrical properties of HB238 thin films has been performed by Böhner *et al.*[35,36].

HB238 belongs to a group of merocyanines that have recently been investigated in literature[34,113,114]. The aggregation behavior can be controlled by exchanging the substituent of the amino group. It was found that the sterical demand of this group determines the aggregation behavior. Large (flexible or bulky) substituents cause J-aggregation, while smaller substituents result in H-aggregates.[114] Being able to precisely control the aggregation behavior in thin films with small chemical modifications, makes this group of molecules an ideal platform to study J- or H-aggregates.

In the present work, HB238 is used as a model system to investigate how molecular order impacts the (strong) light-matter interaction in microcavities. HB238 is an ideal candidate for purpose due to the findings of Böhner *et al.*[35,36] and Weitkamp[37].

Böhner *et al.*[35,36] studied the number of coherently coupled molecules at different annealing temperature of the spin-cast thin films and found that exciton is delocalized over more molecules by increasing the temperature. Weitkamp[37] found that the aggregates can be aligned using seven-atom wide armchair-edge graphene nanoribbons (7-AGNRs), making the optical response polarization-dependent. Therefore, HB238 is an interesting molecule for studying molecular order and orientation. Moreover, molecular aggregates are commonly used in strong light-matter studies[13–15] due to their typically large oscillator strength and sharp spectral features.

3 Experimental methods

During this work, a versatile optical system was built that allows for recording images with either a (confocal) microscope and spectra in both real and reciprocal space. The specimen can be excited with a laser (Chameleon Ultra II with Chameleon Compact OPO-Vis, *Coherent*) that is tunable in the wavelength range 340 - 1600 nm or a halogen lamp in both transmission and reflection mode. Thus, both photoluminescence (PL) and absorbance can be measured. A sketch of the full setup is shown in Fig. 3.7. Details on Fourier-transform spectroscopy and confocal microscopy are given in this chapter. Full details on the sample preparation, measurements and data analysis are given in Sections 4.1, 4.2 and 4.3 in connection with the corresponding studies.

3.1 Fourier-transformation spectroscopy

Spectroscopic methods measure the light intensity as a function of the wavelength. This applies for transmission, reflection and emission spectra. To gain a better understanding of the angular distribution of the interacting light, Fourier-transformation imaging or spectroscopy can be employed. Here, the intrinsic Fourier-transformation properties of lenses are utilized to project an angle-dependent image on a camera or the entrance slit of an imaging spectrometer.[115]

A lens collects emitted, reflected or transmitted light from the sample. The lens then focuses all parallel, plane light waves with the same angle θ to different positions on the back focal plane (see Figure 3.1). In other words, the light emanating from the sample is Fourier transformed from a real space image (spatial function) to a function dependent on the spatial frequencies (angular function) in x- (angular frequency in x-direction: ν_x) and y- (angular frequency in y-direction: ν_y) direction. The angular frequencies describe the propagation direction of the collected light and they are related to the components of the wave vector of light as[42]:

$$\nu_x = \frac{k_x}{2\pi} \tag{3.1}$$

and

$$\nu_y = \frac{k_x}{2\pi}, \tag{3.2}$$

where k_x and k_y are the x- and y-components of the wave vector $k = \sqrt{k_x^2 + k_y^2 + k_y^2} = 2\pi/\lambda$. The x- and y-component of the wave vector can be described by $k_x = k \sin\theta_x$ and $k_x = k \sin\theta_x$, respectively. $\theta_{x/y}$ is the angle between the the z-axis and the x- or y-plane (see Fig. 3.1). A wavefront emanating from the sample in multiple directions can be expressed as the sum of many plane waves corresponding to different spatial frequencies. High spatial frequencies have a large angle relative to the z-axis. A lens, placed

one focal (f) length away from the sample, focuses the plane wave components propagating in one direction to one point in the back focal plane, see Fig. 3.1. In the back focal plane, an image of the angular distribution of the collected radiation is formed. Each point in this image corresponds to the intensity emitted in one direction. Hence, the Fourier transformation imaging is often referred to as back focal plane imaging.[42]

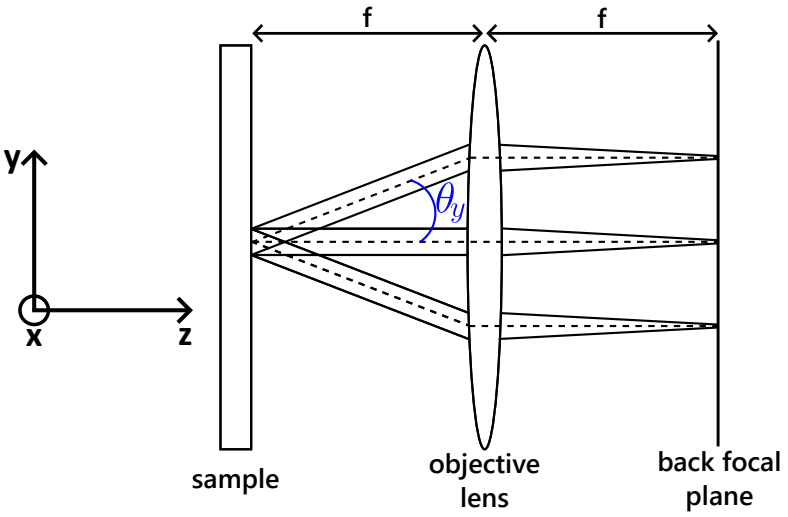

Figure 3.1: Sketch of a sample object one focal length away from an objective lens. Plane waves of light emanate from the sample at multiple angles. The plane waves are collected and parallel light rays with the same angle are focused at the same point in the back focal plane by the objective lens. The angle between the z-axis and an emanated beam is given by θ_y. Concept adapted from Hecht[82].

The maximum angle θ_{max} is limited by the numerical aperture (NA) of the microscope objective. The NA is given by:

$$\mathrm{NA} = n \sin \theta_{max}, \tag{3.3}$$

where n is the refractive index of the sample medium. The larger the NA of the objective lens, the larger the maximum angle that can be collected. Consequently, lenses with large NA are commonly used for Fourier-transformation spectroscopy. High end air objective lenses ($n = 1$) can have an NA of 0.95, which corresponds to a maximum angle of approximately 71.8°. The back focal plane of a microscope objective is often located close to the metal casing of the objective (the focal length f is typically only some millimeters, see Fig. 3.1).[115] As a consequence, further optical components are required to image the back focal plane on a camera or imaging spectrometer.

Fig. 3.2 shows the lens configuration for Fourier transformation spectroscopy that is used in this work. Other possible configurations are detailed by Vasista *et al.*[115]. In short, two lenses with a distance of four focal lengths (4f-correlator) are required to Fourier transform the back focal plane of the microscope objective first back to a real space image after the first lens and then back to the back focal image after a second

lens (see Fig. 3.2). The back focal plane image is then projected on a camera or on a spectrometer slit of an imaging spectrometer for spectroscopic studies.

If a imaging spectrometer is used, the entrance slit can be used as mask to select a thin slice of the back-focal-plane image. This makes it possible to specifically select few angles in one axis and record spectra of all angles parallel to the entrance slit. In this work, angles close to 0° were selected for all measurements. By opening the entrance slit of the imaging spectrometer, it was also possible to observe the back focal plane of the microscope in two dimensions. Depending on the application, it may be beneficial to use more lenses, as reviewed by Vasista *et al.*[115]. In the configuration shown in Fig. 3.2, lens 1 can be removed to measure the real space image or measure spectra without angle-dependent information.

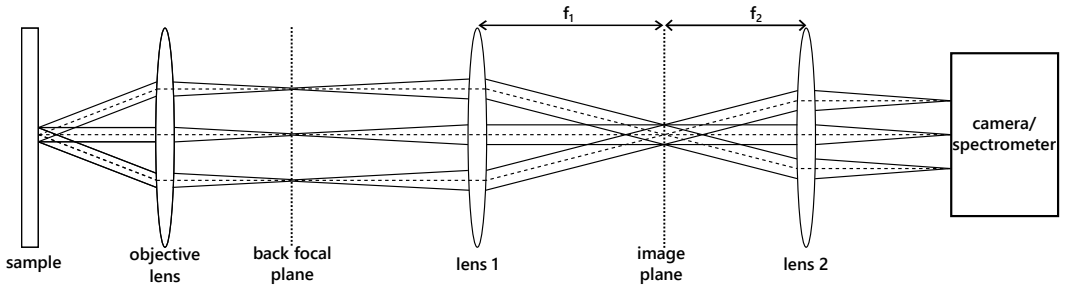

Figure 3.2: Sketch of a lens configuration to record images of the back focal plane of a microscope objective. As shown in Fig. 3.1, all parallel plane light waves are separated by the emission angle in the back focal plane of the microscope objective. Lens 1 Fourier-transforms this to form a real space intermediate image (indicated by a dotted line labeled "image plane"). Lens 2 is added to transform the image into spatial frequencies and separate each angle to different points on a camera or spectrometer. The combination of Lens 1 and 2 forms a 4f-correlator.

The possibility to simultaneously measure the complete radiation pattern has made back focal plane imaging an important tool in many fields in nanophotonics. This method has been applied to directly image the emission patterns of single molecules[116], analyze the scattering at optical antennas[117] and to measure the optical band structure of photonic crystals[118]. Back focal plane imaging is also a proven tool to analyze strong light-matter interaction.[55]

In planar microcavities, the optical path length increases with an increasing angle of incidence, as introduced in Section 2.2. The change in optical path length shifts the spectral position of the confined cavity photon to higher energies. This spectral shift detunes the light-matter interaction between the cavity photon and the excitonic material inside. Therefore, the coupling strength changes and the coupling behavior, e.g. the anti-crossing behavior under strong light-matter interaction, can be analyzed using back focal plane imaging.

The interaction between surface lattice resonances (SLR)s (see Section 2.2.4) and

excitons can also be investigated with Fourier-transformation spectroscopy, as the reciprocal space or the in-plane momentum of the lattice of plasmonic nano-particles is imaged in one shot. Analogue to photonic crystals, an incoming plane wave gets scattered at the ordered particle lattice. Due to constructive and destructive interference, diffraction order (DO)s can be observed when light passes through such a lattice. The DOs can be recorded as a function of the angle with a back focal plane setup. The coupling between the plasmon, the DOs and excitons can then be investigated as a function of the in-plane momentum.[41]

In Fourier-transformation microscopy the relationship between the position of a point in the back focal plane and the direction of the light which is focused at this point is nonlinear (sinusoidal).[119] Therefore, a conversion factor from camera pixel to angle θ has to be determined. This can be achieved by using as sample with known angular scattering, for example a transmission grating can be used. For an incoming plane wave at normal incidence on a grating, the angle θ of the DOs m can be calculated by

$$\theta = \arcsin\left(\frac{m\lambda}{a}\right), \tag{3.4}$$

where a is the period of the grating.[120] By placing a transmission grating in the focal plane of the microscope objective and measuring the Fourier-transformed image by illuminating the grating with a laser with a known wavelength in transmission at normal incidence, the DOs can be observed on the camera or spectrometer (see Fig. 3.3). The center of each spot can be determined by fitting a point spread function to the bright spots. In this work, the ImageJ plugin ThunderSTORM[121] is used. Hence, the angles of the DOs can be calculated with equation 3.4, a sine function with a proportionality factor A (pixel $= A\sin\theta$) can be fitted to the corresponding angle of the DO. With this function camera pixel can be converted to the angle θ.

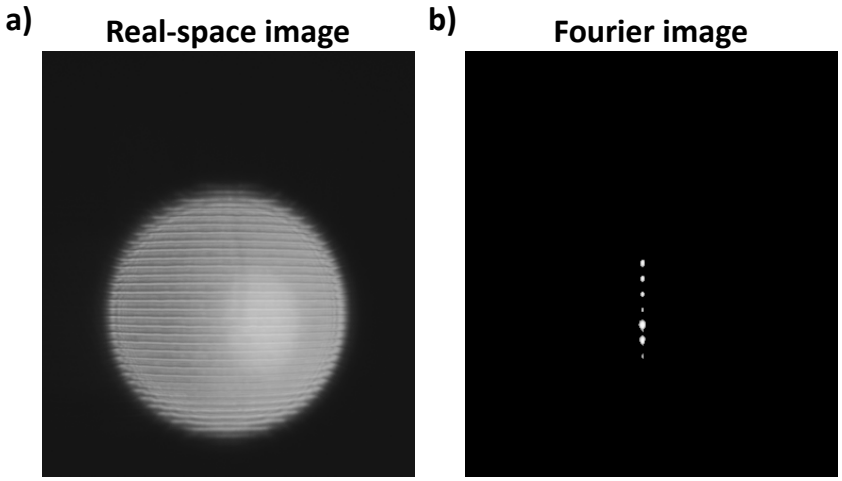

Figure 3.3: a) Shows a real-space image of a commercial transmission grating (GT13-06V, *Thorlabs*). Due to the periodic structure, a plane wave passing through the grating causes diffraction at multiple angles. The diffraction orders are imaged by a Fourier-transform optical setup sketched in Fig. 3.2. The recorded Fourier-transformed image is shown in panel b.

3.2 Confocal microscopy

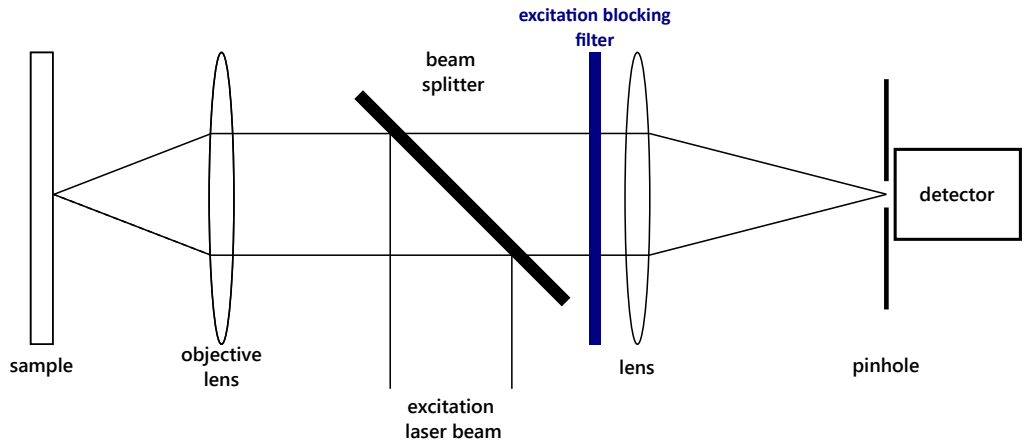

Figure 3.4: Sketch of the optical path of the confocal microscope. The sample is excited with a tightly focused laser beam. The emitted light is collected by a microscope objective. After blocking the excitation light, a second lens focuses the light on the detector. Beams that are not parallel to the optical axis after the objective lens (emission originating from below or above the focal plane), are filtered out by a pinhole in front of the detector.

Confocal microscopy has become a standard method to record high resolution micrographs of objects in sizes close to the diffraction limit with high contrast. In contrast to a conventional microscope, confocal microscopy only detects light emanating from the focal point and the intensity is recorded for each pixel by either moving the sample itself by a nanopositioner or by using a motorized mirror to change the position of the focused beam on the sample. Fig. 3.4 shows the optical sketch of a confocal microscope: A fluorescent sample is illuminated by a tightly focused laser beam through a high NA microscope objective, and the emitted light is collected through the same objective. The emission is separated from the excitation light using a beam splitter or dichroic mirror and any remaining excitation is blocked by an emission filter. The emission is then focused on a detector with a small aperture. In this work, a single-photon counting module (*Micro Photon Devices Srl.*) is used as a detector. By filtering out light that is not emanating from the focal point using the small aperture, the contrast of the image is enhanced.

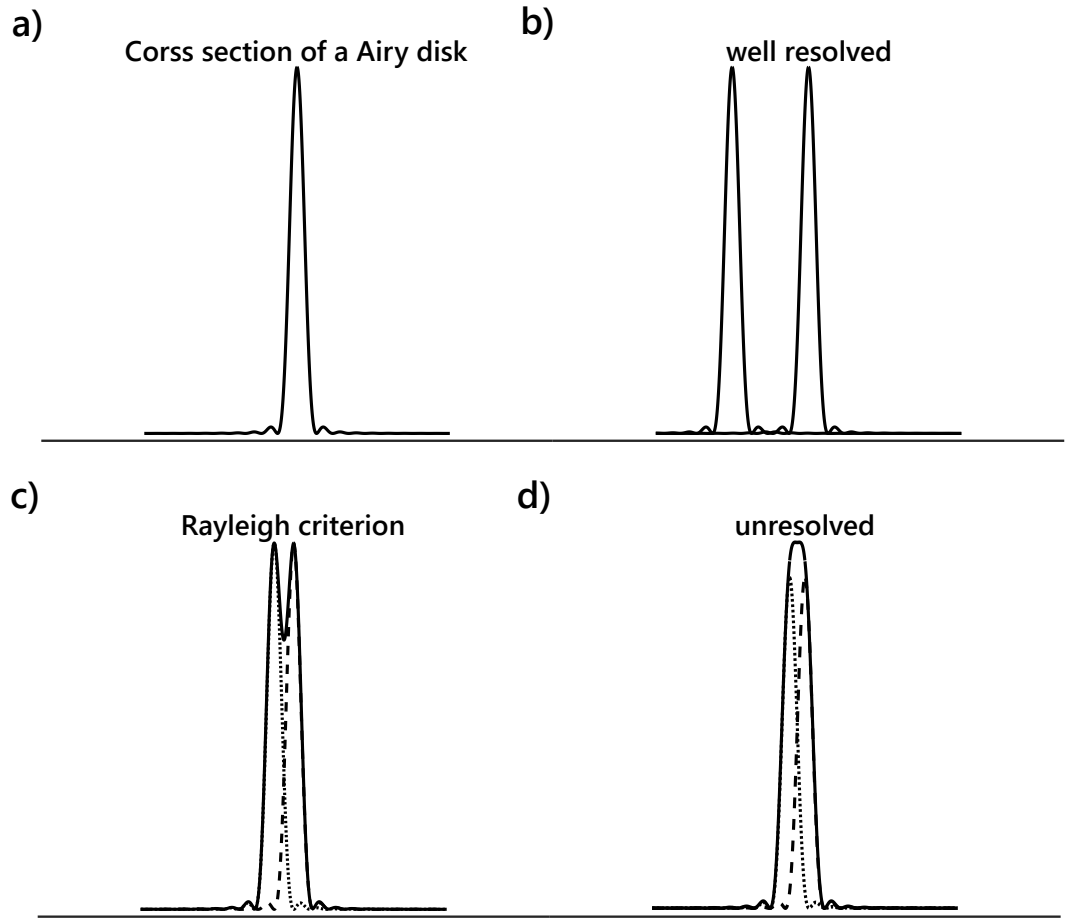

Figure 3.5: a) Cross section of a Airy disk. b)-d) Cross section of two Airy disks in close proximity that b) are well resolved, c) fulfill the Rayleigh criterion, and d) are unresolved. Concept adapted from Hecht[82].

The resolution of the confocal microscope of a fluorescent specimen is defined by the Rayleigh criterion, which states that two point sources can be resolved if the maximum of the point spread function (Airy disk) of the second object is at a distance from the first object equal or larger to the distance at which the point spread function of the first source has a minimum (see Fig. 3.5). Mathematically, the spatial resolution limit r of the confocal microscope is given by

$$r = \frac{0.61\lambda}{\mathrm{NA}}, \tag{3.5}$$

where NA is the numerical aperture of the objective lens.[122][56] This resolution limit is the same as conventional microscopes. The advantage of confocal microscopes is improved contrast by spatial filtering of light that does not originate from the focal plane in the sample. This may be further improved by adding another spatial filter (4f correlator and a pinhole in the focal point of the two lenses) in the detection path. Moreover, by using a piezo controlled scanning technique, the pixel size can be in the range of nanometers, enabling recording diffraction limited images of the specimen.

To record optical images below the diffraction limit, different super-resolution methods have been developed, e.g., stochastic optical reconstruction[123] or scanning near-field optical[124,125] microscopy.

In this work, samples with seven-atom wide armchair-edge graphene nanoribbons (7-AGNRs)s as a template were investigated. These samples have a strong linear polarization dependence. Consequently, two single-photon counting modules are used to to simultaneously image both horizontal and vertical polarized emission to probe the alignment of the templated molecules. In order to measure the same position on the sample with both detectors, care must be taken to align the detectors. For this task, fluorescent micro-spheres (size 0.2 μm) were used to align both detectors to the same fluorescent micro-particle. An example image of two Fluospheres is shown in Fig. 3.6. The position of the particles is identical for both polarizations. Only the intensities are different between the images. This can be attributed to different detection efficiencies between the detectors.

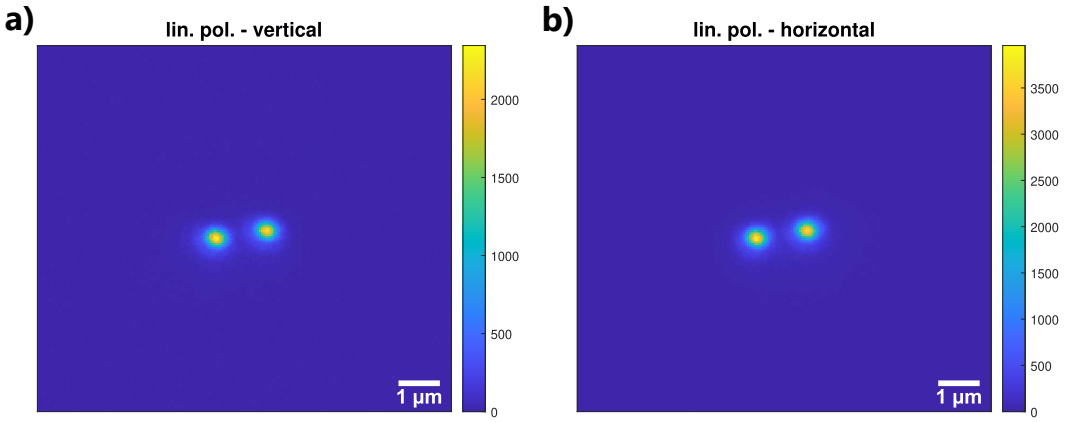

Figure 3.6: Polarization-resolved confocal microscopy images of two dark red fluospheres. The two polarization states were recorded simultaneously with two different detectors. The images for vertically and horizontally polarized light are shown in panel a) and b), respectively.

3.3 Optical setup

The optical setup that was built during this work is sketched in Fig. 3.7. This setup was assembled to offer flexibility: the sample can be excited with a tunable femtosecond pulsed laser system (Chameleon Ultra II with Chameleon Compact OPO-Vis, *Coherent*) with a wavelength range from 340 - 1600 nm (blue path in Fig. 3.7) or a collimated beam from a halogen lamp (not shown in sketch) in both reflection and transmission configuration. More optics, for example polarization optics or filters, can be placed in the excitation path and beam will always be focused to the same spot on the sample due to the active beam stabilizer which corrects for drifts.

The sample can either be analyzed with a microscope (green path in Fig. 3.7), a polarization-dependent confocal microscope (orange path in Fig. 3.7) or by recording spectra. Absorbance (reflection or transmission) and PL spectra can be recorded with a halogen lamp and laser excitation, respectively. If the sample is illuminated with wide-field illumination, i.e., not with a tightly focused beam, multiple spectra can be recorded simultaneously because of the use of an imaging spectrometer (IsoPlaneSCT 320 with a deep-cooled Pixis camera, *Princeton Instruments*).

To switch from imaging the real space to measuring angle-resolved spectra (both in reflection or emission mode), a lens (lens 1 in Fig 3.2) can be added to Fourier-transform the image and to measure the spatial frequencies. After determining a conversion factor from pixel to angle, an angle-dependent measurement from 0° (objective with a NA of 0.95) to $\approx 72°$, can be measured in a single shot (see Section 3.1).

To make the system more adaptable, space for more detectors or optics was left in every optical path. This way, the system can be expanded to account for more measurements in the future. In the current state the versatility of this system allowed the combination of multiple measurements, such as performing confocal microscopy and subsequently measure PL spectra (both angle-resolved or in real space) at points of interest. This was utilized in Section 4.2.

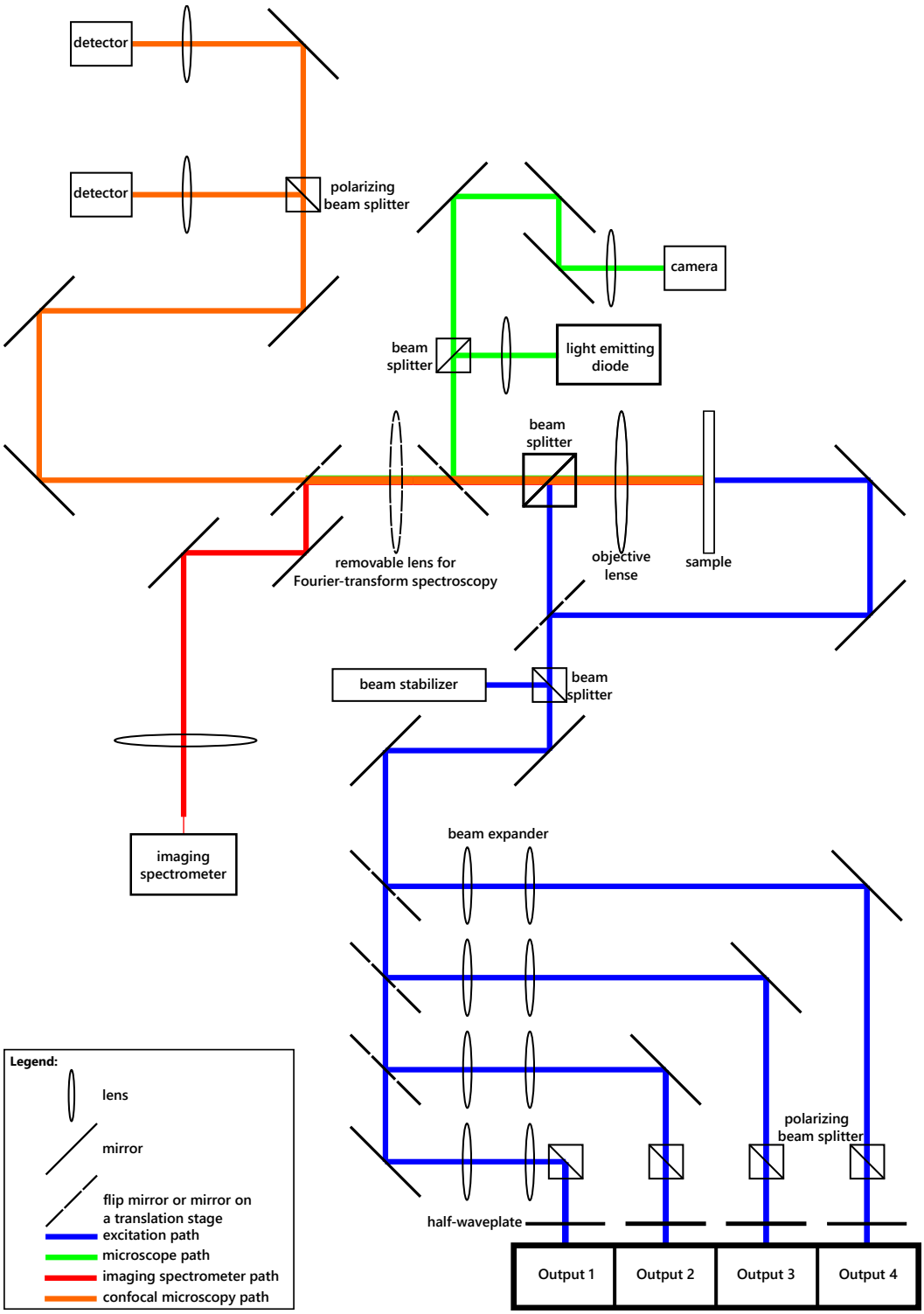

Figure 3.7: Sketch of the optical setup that was built during this work in the current state. Sizes are not for scale.

4 Results and discussion

4.1 Strong light-matter interaction of molecular aggregates with two excitonic transitions

This chapter contains the following publication:

R. Schäfer, L. Böhner, M. Schiek, D. Hertel, K. Meerholz, and K. Lindfors, *ACS Photonics* **2023**, *11*, 111–120.
DOI: https://doi.org/10.1021/acsphotonics.3c01042

In this chapter, we investigate the light-matter interaction in a planar microcavities containing a thin film of HB238. HB238 is a merocyanine that forms molecular aggregates in thin films when spin-cast from solution and subsequent annealing. Due to oblique angle aggregation, both a J- and H-like transition can be observed in absorbance spectra. The spectra show a distinct polarization- and angle-dependence, which indicates that the transition dipole moment (TDM) of the J- and H-transition are parallel and perpendicular to the substrate plane, respectively. The large energy difference between the J- and H-transition of approximately 0.86 eV allows us to simultaneously reach the strong coupling regime for both J- and H-transition with two different cavity modes, resulting in the formation of four polariton states that appear to share the same ground state, because most emission is observed from the polariton with the lowest energy. The light-matter coupling to the H-transition can be switched on or off by polarization, due to the TDM lying parallel to the substrate normal. This polarization dependence makes this system an interesting platform to investigate strong-light matter interaction.

Further, it is investigated, how the light-matter interaction is influenced by the position of the aggregate layer inside the microcavity by varying the thickness of the spacer layers, while keeping the total cavity thickness constant. It was found that the light-matter coupling strength of the J- and H-transition is proportional to in-plane and out-of-plane electric field component, respectively.

The influence of molecular order is also studied in this publication: The molecule-molecule coupling strength can be controlled with the annealing temperature. This can be interpreted as an increase of the number of coherently coupled molecules in the aggregates.[36] The number of coherently coupled molecules is a proxy for the average number of molecules before a defect disturbs the delocalization of the exciton in the aggregates. In planar microcavities, it was found that the light-matter interaction increases with the intermolecular coupling strength: The J-transition is strongly coupled to the cavity mode in the intermediate and strong molecule-molecule coupling regime, while strong light-matter interaction is only observed for strong intermolecular coupling. In other words, an increased molecular order leads to an increase in light-matter coupling strength for HB238.

Author contributions

I have fabricated all samples with some help from the student Riya Sharma for the position-dependent samples. All measurements and data analysis was performed by me with support from Klas Lindfors, with the exception of the ellipsometry of HB238. The manuscript was written in close collaboration with Klas Lindfors and contains contributions from all authors.

4.2 Polarization–controlled strong light–matter interaction with templated molecular aggregates

This chapter contains the following preprint:

R. Schäfer, P. Weitkamp, O. Erdene-Ochir, K. Meerholz, and K. Lindfors, *arXiv preprint arXiv:2503.09798* **2025**.
DOI: https://doi.org/10.48550/arXiv.2503.09798

The revised manuscript was published in:

R. Schäfer, P. Weitkamp, O. Erdene-Ochir, K. Meerholz, and K. Lindfors, *Advanced Optical Materials* **2025**, 13(28), e00998.
DOI: https://doi.org/10.1002/adom.202500998

In this publication, we continue to investigate the influence of order on strong light-matter interaction in planar microcavities: In the previous chapter the influence of dynamic disorder on light-matter coupling was studied. Dynamic disorder results in broadening due to interaction with vibrational modes of the molecules with the delocalized exciton. In that work we investigated light-matter interaction with spin-cast films of HB238, in which the number of coherently coupled molecules can be controlled by annealing temperature (decreasing static disorder with annealing temperature). In the present chapter we now focus on how light-matter interaction is affected by static (orientational) disorder. Here, we use thin films of HB238 that were templated with seven-atom wide armchair-edge graphene nanoribbons (7-AGNRs). The templating induces molecular alignment along the long axis of the 7-AGNRs, resulting in a biaxial crystal. Here, the TDM of the J-like transition is oriented parallel to the 7-AGNRs, and the TDM of the H-like transition is parallel to the substrate normal. This results in a polarization-, angle-of-incidence- and rotation-dependent optical response of the sample: If the electric field component is polarized parallel to the orientation of the 7-AGNRs, the absorption of the J-transition is maximized. If the polarization or the sample is rotated, the absorbance gradually decreases until it is minimized after a 90° rotation. If the sample is illuminated with p-polarized light and non-zero angle of incidence (AOI), a H-like transition arises.

The molecular alignment due to templating results in an increased light-matter coupling strength in the planar microcavity of both the J- (299 meV) and H-transition (190 meV), if the electric field component of the s-polarized light is parallel to the TDM of the J-transition. The coupling strength of the J-transition is strongly reduced to 26 meV, if switched to p-polarized light (electric field component perpendicular to the alignment direction). When the sample is rotated by 90°, the picture reverses and the coupling is maximized with p-polarized, while minimized with s-polarized light. The H-transition can in all cases only be strongly coupled with p-polarized light. At any other rotation angle, polarization splitting into four polaritons is observed for the

J-transition. The polarization splitting and the increased coupling strength parallel to the 7-AGNRs is a direct result of the decrease in orientational (static) disorder.

We utilize this distinct polarization splitting to probe the order of the templated HB238 layer with a combination of polarization-resolved confocal microscopy and subsequent measurement of emission spectra at normal incidence. We find that the HB238 layer is well aligned with only few orientational defects.

Finally, we employ a recently published model[33] to investigate the contribution of gray states on the strong light-matter interaction in the microcavity. The model suggests that the templated HB238 film contains two excitonic species one with increased static (orientational) order that mainly contributes to the light-matter coupling and one with increased dynamic disorder (monomers or aggregates with a small number of coherently coupled molecules), which results in broadening of the J-transition, with a small influence on to the light-matter coupling.

Author contributions

I have fabricated the samples (with exception of the templated HB238 films), built the optical measurement setup (with exception of ellipsometry), performed the optical measurements and analyzed the data (with exception of ellipsometry) with support from Klas Lindfors. I participated in writing and finalizing the manuscript in close collaboration with Klas Lindfors with contributions from all authors.

4.3 Investigation of light-matter interaction between templated molecular layers and plasmonic lattices

4.3.1 Introduction

Confining light to small mode volumes over an extended amount of time increases the coupling between light and matter. If the interaction strength is large enough, the strong coupling regime is reached. In this regime, the light-matter interaction exceeds the total losses of the system and the re-absorption of photons by the material becomes the dominant process. Here, hybrid light-matter states are formed, called polaritons.[12] Polaritons have properties of both the light and the matter component, which has lead to interesting observations in recent studies, such as improved energy transport in transistors[73–75], lasing at room temperature[80], and modified chemical reaction rates[71,72]. Systems that confine light and materials with large oscillator strength are required to reach the strong coupling regime. Strong coupling has been demonstrated in a multitude of geometries, such as planar microcavities[80], micropillars[19], microdisks[20] and photonic crystals[18]. In recent years, plasmonic lattices have gained interest in studying light-matter interaction, due to the formation of surface lattice resonances (SLR). These are sharp modes that form by a collective coupling between nano-particles ordered in an array with a lattice period on the order of magnitude of the wavelength of the light. Due to this collective coupling, the photons are confined which results in an increased light-matter coupling. This has been used to study strong coupling[17], long-range energy propagation[77], and for biosensing applications[126].

Strong coupling between plasmonic lattices and organic molecules has mostly been studied with disordered materials.[17,127–129] Recently, it was shown for planar microcavities that molecular alignment can lead to a larger coupling strength, which is a important parameter for, e.g., polariton lasing. For plasmonic lattices, it has been shown that an anisotropic single crystal of tetracene can be used to control the light-matter coupling strength from the weak- to the strong-coupling regime.[30] Ordered excitonic components are thus highly interesting for studies of light-matter coupling in plasmonic lattices.

In this work, we investigate the influence of order on coupling between plasmonic lattices and ordered molecular layers. We study both the influence of dynamic and static disorder. Dynamic disorder results in broadening of the absorption line by overlap of the exciton and molecular vibrations in molecular crystals, while static disorder describes, e.g., the orientation of molecules (orientational disorder). Here, we use the merocyanine dye 2-[5-(5-dibutylamino-thiophen-2-yl-methylene)-4-*tert*-butl-5*H*-thiazol-2-ylidene]-malononitrile (HB238[34]) as a model system. Merocyanines are a class of molecules that tend to form molecular aggregates.[94] The aggregation can result in a red-shifted (J-aggregate), blue-shifted (H-aggregate), or the appearance of both a red- and a blue-

shifted absorption relative to the monomer. J- and H-aggregates are formed by "head-to-tail" and "side-by-side" arrangement of the molecules, respectively.[94,95,105,106] In the case of HB238, the molecules aggregate in oblique angle configuration, resulting in both an J- and a H-like spectral transition.[35,36,112] In a recent publication we have shown that both the J- and the H-transition can be strongly coupled in planar microcavities (see Sections 4.1 and 4.2). In amorphous (spin-cast) thin films of HB238, the transition dipole moment (TDM) of the J-transition is parallel to the sample plane, but has no defined direction. Here, we use seven-atom wide armchair-edge graphene nanoribbons (7-AGNRs) as a template to orient the TDM of the J-transition to study and control the light-matter interaction with plasmonic lattices.

4.3.2 Results and discussion

We investigate the light-matter interaction between a plasmonic gold lattice that supports SLR modes with aligned (templated) molecular layers of HB238. The system is sketched in Fig. 4.1a. The optical properties of the two components (SLR and HB238) are detailed in Sections 2.2.4, 2.3.1, and 4.2. In short, the molecule HB238 belongs to a group of merocynanines that have been studied due to their ability to form aggregates in thin films displaying J- or H-transitions.[34,113,114] HB238 molecules aggregate in oblique angle fashion, resulting in both a J- and H-like transition, with the TDM of the J- and H-transition aligned parallel and perpendicular to the substrate plane, respectively. Due to the fascinating physical properties properties, HB238 has been intensively studied.[35–37,112,130–134] Weitkamp[37] demonstrated that the molecular crystals can be aligned by physical vapor deposition on 7-AGNRs. The 7-AGNRs serve as a template for the molecular aggregates, inducing uniaxial growth parallel to the long axis of the 7-AGNRs.[37] This results in a highly polarization dependent response: if the electric field of light is parallel to the 7-AGNRs' long axis, the absorption of the J-transition at 1.65 eV is observed as shown in Fig. 4.1b. The signal strongly decreases, if the sample or polarization is rotated by 90° (see Fig. 4.1b). Note that the TDM of the H-transition is parallel to the substrate normal and therefore not accessible at normal incidence. For the templated layer, the H-transition can still be observed at non-normal angle of incidence (AOI) and p-polarized light (see Sections 4.1 and 4.2).

In Section 4.2 we studied the influence of the alignment on strong light-matter interaction in a planar microcavity. The molecular alignment results in the observation of polarization splitting of the polaritons, with increased Rabi spitting compared to a non-templated film, if the electric field component of light is parallel to the 7-AGNRs long axis. In the perpendicular case, the coupling strength is minimized. If the cavity is rotated by any other angle, all four polaritons are observed. This polarization splitting allowed us to spatially probe the quality of alignment and the influence of

order on light-matter interaction.[132] Here, we investigate the coupling between SLR and templated HB238. The SLR are the collective coupling between localized surface plasmon resonances (LSPR) of plasmonic nano-particles in a periodic lattice with the diffraction order (DO) of the array, resulting in sharp resonances with large Q-factors as illustrated in Fig. 4.1c. The SLR allow for a multitude of geometries such as square, rectangular, hexagonal[41] or superlattices[135] with tailored light fields, which makes SLR an interesting platform to study light-matter interaction with ordered molecular layers. In literature, disordered molecules[17,127–129] are typically used for light-matter studies involving plasmonic lattices. Recently, Berghuis *et al.*[30] investigated the interaction between a silver nano-particle array and a tetracene single crystal, which has anisotropic optical properties. The study includes the rotation of the crystal on the lattice, which allows for controlling the coupling strength from weak to strong, depending on the rotation angle.[30]

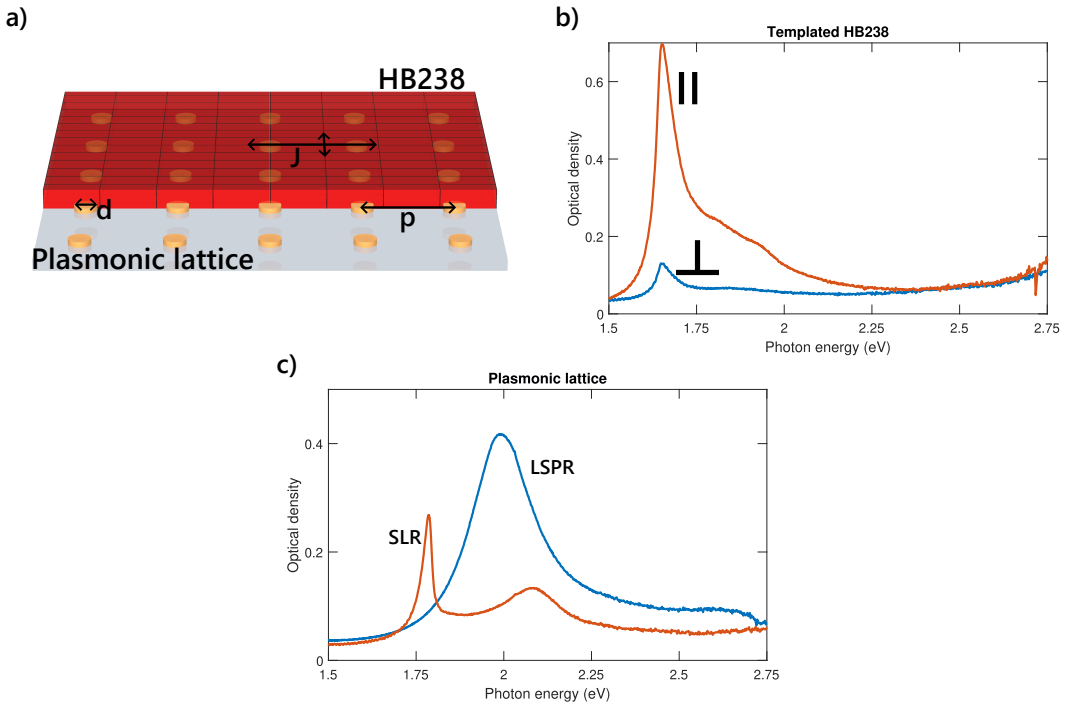

Figure 4.1: a) Sketch of the investigated system: Plasmonic lattices with particle spacing p and diameter d. A aligned layer of HB238 is deposited on the lattice. The molecular alignment is achieved by templating by graphene nanoribbons. b) Transmission spectra of the templated HB238 film parallel (∥) and perpendicular (⊥) to the graphene nanoribbons. c) Transmission spectra of localized surface plasmon resonances mode from a subdiffractive lattice (period: 300 nm) and of a surface lattice resonances mode.

The plasmonic array consists of gold nano-disks with a diameter of 92 nm and a height of 50 nm. Arrays with different periods were studied in order to shift the SLR spectrally. We first characterize the lattice without the excitonic layer of HB238. A homogeneous refractive index environment is achieved by spin-casting a few hundred nanometers thick layer of polyvinyl alcohol (see Methods for full details), which

is required for sharp SLR modes at normal incidence (see Section 2.2.4). To detune the photonic mode, we fabricated lattices with periods in the range of 415 - 535 nm. A representative scanning electron micrograph of an array is shown in Fig. 4.2a. In Fig. 4.2 we display the transmission spectra as a function of the inverse lattice spacing $k = 2\pi/p$, where p is the (real space) lattice period, following the approach of Väkeväinen *et al.*[17]. Clear anti-crossing is observed between the LSPR and DO. From now on the sharper and lower energy signal of the two formed modes will be referred as SLR. The coupling can be described by a two-oscillator Hamiltonian[17,136]

$$H = \begin{pmatrix} E_{\mathrm{LSPR}} & g_1 \\ g_1 & E_{\mathrm{DO}} \end{pmatrix}, \tag{4.1}$$

with the LSPR energy E_{LSPR} and the DO energy at normal incidence E_{DO}, respectively. The interaction strength is given by the coupling parameter g_1. E_{DO} is dependent on the effective refractive index of the medium n_{eff} and the lattice period

$$E_{\mathrm{DO}} = \frac{\hbar c}{n_{\mathrm{eff}}} \frac{2\pi}{p}. \tag{4.2}$$

The fit by diagonalizing the Hamiltonian yields a coupling strength of approximately 130 meV between the DO and the LSPR. Note that the coupling parameter g_1 is half of the Rabi energy ($\hbar\Omega = 2g_1$).

Now we turn to the investigation of light-matter interaction between the SLR and spin-cast HB238 (see Fig. 4.2). Note that a few hundred nanometers thick layer of polyvinyl alcohol was spin-cast on the HB238, because the approximate 20 nm HB238[36,112] layer is not sufficient to achieve a homogeneous refractive index environment to form sharp SLR modes at normal incidence. In this case, four signals are observed: one period-independent peak at 1.65 eV, which corresponds to the J-transition of HB238, indicating that not all aggregates are coupled or are only weakly coupled to the SLR mode. The other three signals show dispersion with the respect to the lattice spacing and display clear anti-crossing behavior, indicating strong light-matter interaction. Three new eigenstates have formed by the interaction between the LSPR, DO and HB238: a lower, middle and upper polariton. We use a three coupling oscillator model[17], in order to quantify the coupling strength:

$$H = \begin{pmatrix} E_{\mathrm{LSPR}} & g_1 & g_2 \\ g_1 & E_{\mathrm{DO}} & g_3 \\ g_2 & g_3 & E_{\mathrm{HB238}} \end{pmatrix}, \tag{4.3}$$

where g_2 and g_3 quantify the coupling between the LSPR and the J-transition (with energy E_{HB238}) and the coupling of the DO and J-transition, respectively. A fit of

the eigenenergies obtained by diagonalizing the Hamiltonian Equation 4.3 to the data, shows good agreement (see Fig. 4.2c). The best fit yields approximately 105 meV for g_1 (SLR mode) and 112 meV for g_3 (coupling of HB238 to the SLR mode). The parameter g_2 is close to 0 meV, due to the large energy difference between the LSPR (≈ 2 eV) and HB238 (1.65 eV). Therefore, the dispersion of the upper polariton is shifted to similar energies as in the case without HB238 (compare Fig. 4.2b and c).

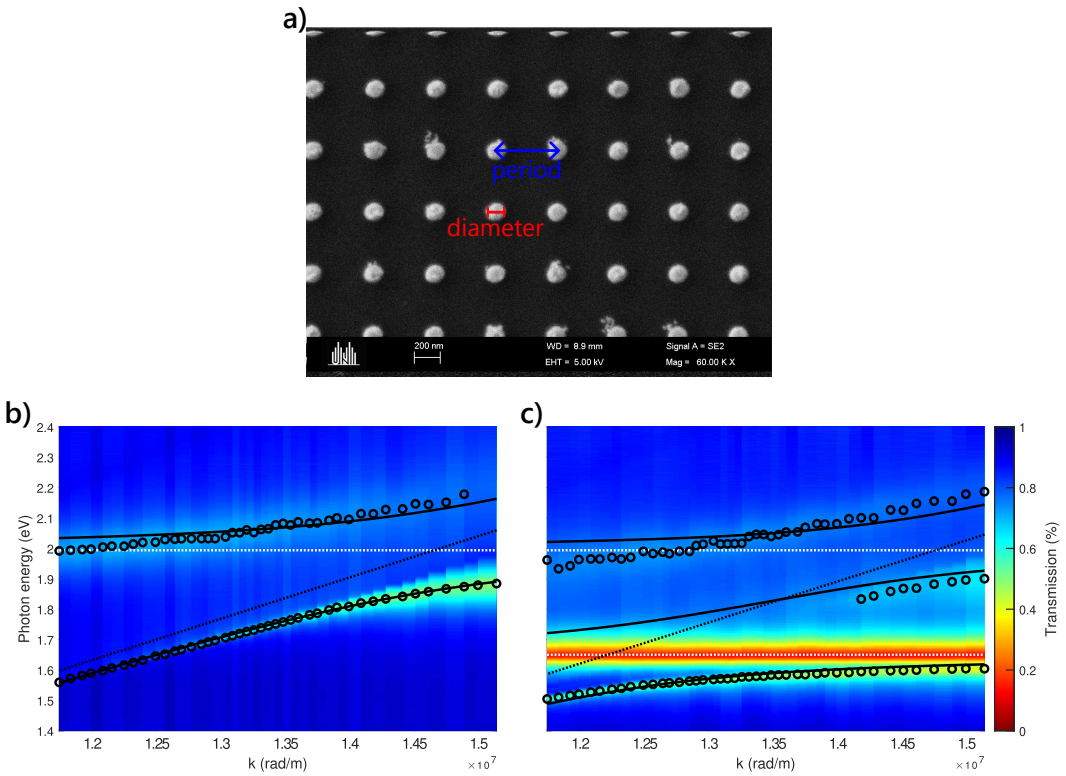

Figure 4.2: a) Scanning electron micrograph of a gold nano-particle lattice with a diameter of approximately 92 nm and a period p of 475 nm. b) and c) Transmission spectra as a function of the inverse lattice spacing $k = 2\pi/p$ of lattices covered with polyvinyl alcohol and lattices coupled to HB238, respectively. Black circles indicate the measured spectral peak positions. The horizontal white dotted lines at approximately 2 eV and 1.65 eV is the localized surface plasmon resonances of the gold particles (panel b and c) and the J-transition of HB283 (panel c), respectively. The black dotted line is the calculated position of the diffraction order (see Equation 4.2) and the black solid lines are the fit results from the coupled oscillator models, Equation 4.1 and 4.3.

We have thus demonstrated that the strong coupling regime can be reached by the interaction between SLR and spin-cast HB238. We now continue exploring the light-matter interaction with templated HB238 layers. The oriented TDM of the transitions in templated layers offers much potential for engineering the light-matter interaction in SLR. A dark-field microscope image of the sample is shown in Fig. 4.3a, displaying a homogeneous layer of HB238, with the exception at the top left of Fig. 4.3a, where cracks and defects can be seen. More dark-field imates and atomic force micrographs of the sample are shown in the Appendix A.3.

The 7-AGNRs were carefully aligned parallel to one of the lattice edges. In the spectroscopic experiments the sample was aligned such that the horizontal polarization is perpendicular to the 7-AGNRs. Fig. 4.3b shows the transmission spectra for horizontally polarized light. In this case, the electric field is perpendicular to the J-transition of HB238 (see Fig. 4.1b). Even though the absorption of the J-transition is minimized in this configuration, the light-matter interaction is large enough to reach the strong coupling regime. The coupling strength between the SLR and HB238 was determined as approximately 39 meV, by using the three coupled oscillator model (Equation 4.3).

If the electric field is polarized parallel to the 7-AGNRs, the light-matter interaction increases to approximately 88 meV. Interestingly the coupling strength is only doubled, while the extinction ratio (determined from the peak maxima) in the thin film is almost a factor of six between the two polarizations (see Fig. 4.1b). Also in the parallel case, the coupling strength is lower than if HB238 is spin-cast (compare Fig. 4.2c and Fig. 4.3c). For a qualitative comparison, finite element simulation was employed with the complex biaxial refractive index of HB238 from Section 4.2 (see Fig. 4.3d and e). Both the perpendicular (Fig. 4.3d) and parallel (Fig. 4.3e) case agree well with the experimental data: The lowest polariton clearly displays anti-crossing behavior with the HB238, while displaying a similar dispersion strength as the experimental data, indicating similar coupling strength. The reduced coupling strength in going from spin-cast to templated HB238 film may be a result of aggregates with a low number of coherently coupled molecules which lead to a broadening of the J-transition (see Fig. 4.1b and Section 4.2). Therefore, not all oscillator strength lies in the J-transition, ultimately reducing the number of aggregates coupled to the SLR. This result is in stark contrast to the increased light-matter interaction between planar microcavitites and templated HB238 in Section 4.2 due to the molecular alignment. It seems that in planar microcavities the static disorder plays a larger role for the light matter interaction, while dynamic disorder dominates the coupling strength in plasmonic lattices. Further studies may reveal a more detailed picture of the optical processes involved.

Surprisingly, the middle polariton is not clearly visible in Fig. 4.3e, while the other spectral features agree well with Fig. 4.3c. This may also be a result of the broadened J-transition in the templated HB238 film: Because not all aggregates are strongly coupled to the SLR, the J-transition is visible in transmission spectra of HB238 films on plasmonic lattices (in contrast to the results with microcavities in Section 4.1 and 4.2). The spectra of the uncoupled or weakly coupled aggregates therefore overlap with the middle polariton, which results in reduced visibility of the middle polariton.

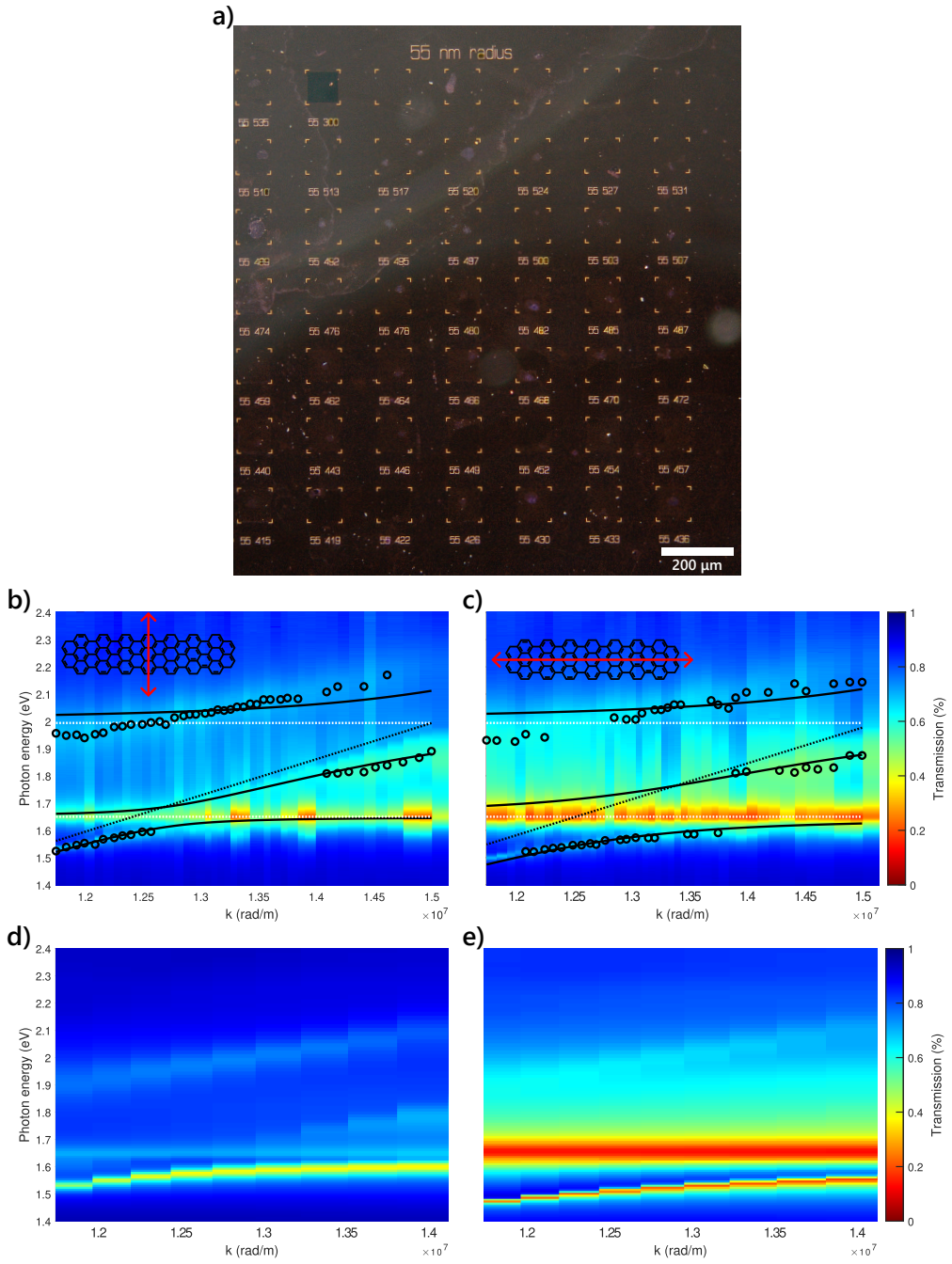

Figure 4.3: a) Dark-field microscope image of gold lattices with a templated HB238 layer. The nominal radius is 55 nm, which corresponds to a diameter of approximately 92 nm. The second number under each lattice index is the lattice period. b), c) Measured transmission spectra of gold nano-particle lattices coupled with a templated HB238, for the electric field perpendicular (panel b) and parallel (panel c) to the graphene nanoribbons. The horizontal white dotted lines at approximately 2 eV and 1.65 eV are the localized surface plasmon resonances of the gold particles and the J-transition of HB283, respectively. The black dotted line is is the calculated position of the diffraction order (see Equation 4.2) and the black solid lines are the fit results from three coupled oscillators model. d), e) Simulated transmission spectra of gold nano-particle lattices with templated HB238. k is the inverse lattice period ($k = 2\pi/\text{period}$).

4.3.3 Conclusion

To conclude, we investigated the light-matter interaction between plasmonic lattices and HB238. HB238 aggregates in oblique angle configuration, with the TDM of the J-like transition parallel to the substrate plane and the TDM of the H-like transition parallel to the substrate normal. Therefore, only the J-transition is optically accessible with measurements at normal incidence. Molecular alignment with 7-AGNRs as a template results in a highly polarization dependent response, with strong absorption at 1.65 eV, when the electric field component of light is parallel to the alignment direction. The intensity drops by a factor of almost six, when the electric field is polarized perpendicular to this. These optical properties make (templated) HB238 an interesting system to investigate strong light-matter interaction. In this study we used plasmonic lattices to confine light to a small mode volume for an extended amount of time to reach the strong coupling regime.

Plasminc lattices support SLR modes by coupling the DO of the lattice with the LSPR of plasmonic nano-particles. We fabricated gold nano-disk lattices with a LSPR mode at approximately 2 eV and periods in the range of 415 and 535 nm. The resulting SLR mode lies in an energy range to couple to the J-transition of HB238. By spin-casting HB238 (TDM of the J-transition randomly oriented in the lattice plane), the strong coupling regime was reached with a coupling strength of approximately 112 meV.

With molecular alignment by 7-AGNRs, we expect increased and reduced coupling strength by exciting molecules parallel and perpendicular to the alignment direction, respectively. Instead, the light-matter interaction was reduced in both cases, compared to the spin-cast case. If the electric field component and the aligned molecules are perpendicular to each other, the coupling strength is approximately 39 meV. In the parallel case, the coupling strength reaches a value of approximately 88 meV. The polarization dependence of the coupling strength confirms molecular alignment, but the overall reduction of the light-matter interaction might be caused by increased dynamic disorder. The increased disorder can be observed by the broadened J-transition in the thin-film transmission spectrum. Finite element simulations reproduce the experimental data well. Due to these unexpected results, the light-matter interaction between templated molecules and SLR seem non-trivial and require further investigations with, e.g., other lattice geometries, such as anisotropic nano-particles, rectangular, or hexagonal lattices. The results may be used to further study the molecular order. Getting a better understanding of the molecular order may make molecular templating a feasible method to tune the optical properties for organic optoelectronics. The strong polarization dependent response of the coupling strength is already a promising property for polarization sensitive applications such as polarizers.

4.3.4 Methods

Fabrication of plasmonic lattices

Plasmonic lattices were fabricated by electron beam lithography on borosilicate glass substrates (D263 T, *Präzisions Glas & Optik GmbH*). The structures were exposed with an electron beam with a 225 μC/cm^2 dose on a double layer of poly(methyl 2-methylpropenoate) (AR-P 642.04 and AR-P 672.02, *Allresist*). To prohibit charging, a layer of a electron conducting polymer (ESpacer 300Z, *Showa Denko*) was deposited on the resist. The bottom layer (AR-P 642.04, *Allresist*) has a thickness of 150 nm, followed by a second layer of 50 nm (AR-P 672.02, *Allresist*). The bottom layer, electron sensitivity is larger than that of the top layer, resulting in a undercut after development in a methyl isobutyl ketone/isopropanol solution (1:3 volume ratio). 3 nm of titanium and 50 nm of gold was subsequently evaporated via thermal physical vapor deposition. The metal on the polymer was removed with a lift-off procedure in dimethylsuccinat (AR 300-76, *Allresist*). Lattices with periods from 415 to 535 nm and 300 nm were fabricated. The size for all lattices was 90×90 μm. For a homogeneous refractive index around the particles, an approximately 320 nm thick layer of polyvinyl alcohol was spin-cast from a water solution on either the plasmonic lattice or HB238.

Spin-cast HB238 layer

100 μl of HB238/Chloroform solution with a concentration of 1×10^{-2} mol/l was spin cast on the plasmonic lattice, yielding a thin layer of approximately 20 nm.[36,112] The substrate was then annealed at 140 °C to induce aggregation of the molecules.

Synthesis and transfer of seven-atom wide armchair-edge graphene nanoribbons

For the synthesis and transfer of 7-AGNRs the same protocol as in Section 4.2 was used: 7-AGNRs were synthesized on a clean Au(788) single crystal in ultra high vacuum by deposition of 16 Å of 10,10-dibromo-9,9-bianthryl and subsequent heating to 200 and 400 °C. The 7-AGNRs film was transferred from the gold crystal to the plasmonic lattice sample, by first covering the 7-AGNRs layer with poly(methyl 2-methylpropenoate) and delaminating the 7-AGNRs with the poly(methyl 2-methylpropenoate) by the bubble transfer method[137]. The delaminated film was washed trice, and then placed on the plasmonic lattice substrate while carefully aligning the 7-AGNRs parallel to a lattice axis and dried for 24 h. The sample was subsequently placed in boiling acetone to remove the poly(methyl 2-methylpropenoate) layer. The synthesis and transfer of 7-AGNRs was done by Manuel Neubauer.

HB238 deposition on 7-AGNRs

A 25 nm thick layer of the molecule HB238 was deposited with thermal physical vapor deposition with a rate of 0.03 Å/s while heating the substrate to 74 °C under high vacuum conditions. Atomic force microscope images (MFP-3D Infinity AFM, *Oxford In-*

struments Asylum Research) were recorded in alternating contact mode using AC200TS tips (*Olympus*) to investigate the alignment. The atomic force micrographs were analyzed using the Gwyddion software[138]. The evaporation of HB238 and atomic force microscopy was performed by Manuel Neubauer.

Transmission spectra

Transmission spectra were recorded by illuminating the sample with a halogen lamp from the back of the substrate. The light is collected with a 4x microscope objective (UPlanFL N, *Olympus*) with an numerical aperture (NA) of 0.13. Therefore, the objective only collects small angles. The transmitted light is analyzed with a broadband linear polarizer (UBB01A, *Moxtek*) and recorded by focusing the light on the spectrometer entrance slit of an imaging spectrometer (IsoPlaneSCT 320 with deep cooled Pixis camera, *Princeton Instruments*). The arrays were selected by using the imaging capabilities of the spectrometer and incrementally moved by the motorized stage to the next array. Multiple spectra from each lattice were averaged to increase the signal to noise ratio. Reference spectra were measured with the sample removed.

Data analysis

The transmission spectra were analyzed and visualized with Matlab (*MathWorks*). First multiple spectra form the same lattice were averaged to achieve a better signal to noise ratio, followed by dividing the measurements with the spectrum of the halogen lamp (measured with no sample). The minima in the transmission spectra were identified with a peak finding function, and the minima were subsequently fitted with a two- or three oscillator model using the trust-region-reflective algorithm. A subdiffractive lattice (lattice spacing 300 nm) was used to determine the LSPR spectral position.

Finite element simulations

The finite element simulations were performed with the Wave Optics module in frequency domain (COMSOL Multiphysics, *COMSOL Multiphysics GmbH*) to simulate transmission spectra the geometry is sketched in Fig.4.4. A gold cylinder with 40 nm height, 46 nm radius and refractive index from Johnson and Christy[139] was placed on a substrate with constant refractive index of 1.52. A layer with the templated biaxial HB238 complex refractive index[132] with 30 nm thickness was placed around the particle. A homogeneous refractive index environment was achieved by implementing another layer on top of HB238 with a refractive index of 1.47 corresponding to polyvinyl alcohol. The lattice was simulated by setting periodic boundary conditions (Floquet periodicity) along the substrate surface. Lattices with periods from 415 - 535 nm were simulated.

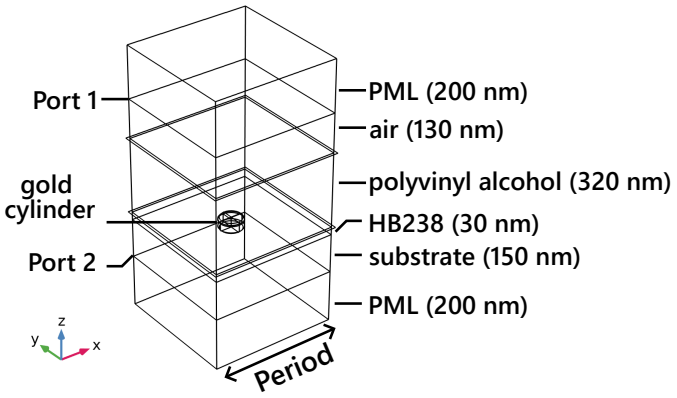

Figure 4.4: Geometry for the finite element simulations. A plane light wave was launched at port 1 and collected at port 2. Periodic boundry conditions were implemented along the cuboid faces along the x- and y-plane. At the top and bottom a perfectly matched layer (PML) was placed with a refractive index of 1 and 1.52, respectively. The PMLs mimic a non-reflective infinite space by perfectly absorbing all light waves.

Author contributions

I have fabricated the plasmonic lattices and the samples with a spin-cast HB238 layer. I measured and simulated the transmission spectra, and analyzed the data. The graphene nanoribbons were synthesized and transferred by Manuel Neubauer (Meerholz group, University of Cologne), who also deposited HB238 on these samples. M.N. measured and analyzed the atomic force micrographs. Klas Lindfors helped with the simulations and measured the scanning electron micrographs. Initial planning and introduction to the simulations were obtained during my three month research stay in the group of Prof. Tommi Hakala (University of Eastern Finland, Joensuu, Finland).

5 Conclusion and outlook

In this work, the influence of molecular order on light-matter interaction was studied. For this purpose, the molecule HB238 was used as a model system, because both dynamic and static disorder can be controlled in thin films. For the light-component both planar microcavites and plasmonic lattices were investigated, with vastly different results.

First, a spin-cast thin film of HB238 was incorporated in a planar microcavity. HB238 forms oblique angle aggregates that show both a J- and H-like transition in transmission spectra, with the transition dipole moment (TDM) of the J-transition in the sample plane and the H-transition perpendicular to the sample plane. In a microcavity, both transitions can be simultaneously addressed with two separate cavity modes, resulting in the formation of four polaritons. The J-polaritons can be observed with both s- and p-polarized light, while the H-polaritons are optically only accessible with p-polarized light, making the system a fascinating platform to investigate strong coupling behavior. The polarization-dependent strong light-matter coupling may also be interesting for polarization optics.

In a further study, the influence of dynamic disorder was studied by using films with different levels of aggregation: the number of coherently coupled molecules and therefore the order increases with annealing temperature of spin-cast films of HB238. In the microcavity, the light-matter interaction can be controlled from weak to strong for both the J- and H-transition with increased molecular order. More ordered films are necessary to reach the strong-coupling regime for the H- than for the J-transition. A possible reason for this is, that the H-transition is stronger effected by dynamic disorder due to being shifted to spectral regions with overlap to the vibrational states of the monomer, resulting in spectral broadening.

The influence of static disorder on light-matter interaction was investigated by orienting the TDM of the J-transition of HB238 parallel to aligned seven-atom wide armchair-edge graphene nanoribbons (7-AGNRs) as a template, resulting in polarization and orientation dependence of the J-transition in the bare thin film. For the templated HB238 layers, the light-matter coupling strength decreases or increases in planar microcavities for the J-transition, if the system is excited with the electric field perpendicular or parallel to the TDM of the J-transition, compared to the spin-cast system. This is in agreement with previous theoretical and experimental studies with other systems, where alignment resulted in an increased coupling strength. In these studies, aligned polymers or single-crystals were used. Both require complicated case-by-case solutions to achieve alignment, or high quality crystals that can be used in microcavities. Using 7-AGNRs as templates is a relatively universal method to achieve molecular alignment in thin films. This may result in future use for polaritonic devices, such as polariton

organic light emitting devices or polariton lasers.

The orientational order was further studied by polarization-resolved emission micrographs in a planar microcavity. Here, we take advantage of polarization splitting that occurs when the molecular crystal is excited at an arbitrary angle that is not parallel or perpendicular to the alignment. If polarization splitting occurs, four polaritons around the J-transition energy are observed. Our findings confirm near-perfect molecular alignment along the 7-AGNRs in the microcavity.

Transmission spectra of bare films of templated HB238 show increased dynamic disorder evident by spectral broadening in the region of the monomer. The states responsible for the broadening become optically dark or gray under strong light-matter coupling. The contribution of these states was investigated by employing a recently published multi-oscillator method[33]. By applying this model we found that mainly one polariton is responsible for the strong coupling behavior in the microcavity. This can be interpreted as an increase in order under strong light-matter interaction. These results emphasise that aligned 7-AGNRs can be utilized as molecular templates to increase strong light-matter coupling for future optoelectronic devices.

In the last study, the light-matter interaction between HB238 and plasmonic lattices was investigated. Plasmonic lattices can be fabricated in multiple different geometries, such as square, rectangular, hexagonal, or as super lattices. This makes them an interesting platform to investigate light-matter interactions. Here, square gold nano-cylinder lattices were fabricated to study the coupling with aligned HB238 aggregates. The alignment results in a polarization-dependent response of the strong-coupling behavior (coupling strength maximized along the TDM of the J-transition, minimized perpendicular to the TDM of the J-transition). Interestingly, the coupling strength with excitation parallel the aligned aggregates is smaller than when HB238 is spin-cast on the sample, which is a vastly different result than for planar microcavities. These results indicate that large dynamic order is more important than static order for plasmonic lattices, while the opposite is true for planar microcavities. This conclusion needs further confirmation by for example studying the light-matter interaction with spin-cast HB238 that was annealed at different temperatures, other templates, or different plasmonic lattice geometries.

The insight on light-matter interaction with ordered molecular structures may also be useful for the Research Training Group 2591 - Template-designed Organic Electronics (TIDE). In TIDE, molecular templating is explored from the synthesis of molecules to the theoretical framework for (opto-)electronic devices. In this work the optical side of molecular order in microcavities has been investigated. Combining these optical properties with electronics (e.g., organic light emitting diodes) may result in improved device performance.

Part of this thesis was also the development of a versatile optical setup that incor-

porates all optical methods used in this work. With this setup it is possible to record transmission, reflection and emission spectra in both real space and in Fourier-space (angle-dependent), images and polarization-resolved confocal micrographs. All methods can be combined to gain more information about the sample. The setup's versatility allowed students from the working group of Prof. Meerholz to locally probe the polarization of a chiral polymer and will be used by other group members in the future. The setup can also be expanded for the use of more detectors or for the combination of optical with electric measurements.

The theoretical and fabrication (design and nano-fabrication) framework was established in the working group for plasmonic lattices. Plasmonic lattices are a great platform to increase light-matter interaction or to stir light. This may be used for chiral lattices or plasmonic lattices can be combined with other systems, such as planar microcavities to further enhance the light-matter interaction.

A Appendix

A.1 Supporting information: Strong light-matter interaction of molecular aggregates with two excitonic transitions

This chapter contains the Supporting Information of the following publication:

R. Schäfer, L. Böhner, M. Schiek, D. Hertel, K. Meerholz, and K. Lindfors, *ACS Photonics* **2023**, *11*, 111–120.
DOI: https://doi.org/10.1021/acsphotonics.3c01042

A.2 Supporting information: Polarization–controlled strong light–matter interaction with templated molecular aggregates

This chapter contains the Supporting Information for the following preprint:

R. Schäfer, P. Weitkamp, O. Erdene-Ochir, K. Meerholz, and K. Lindfors, *arXiv preprint* **2025**.
DOI: https://doi.org/10.48550/arXiv.2503.09798

The revised Supporting Information was published in:

R. Schäfer, P. Weitkamp, O. Erdene-Ochir, K. Meerholz, and K. Lindfors, *Advanced Optical Materials* **2025**, 13(28), e00998.
DOI: https://doi.org/10.1002/adom.202500998

A.3 Investigation of light-matter interaction between templated molecular layers and plasmonic lattices

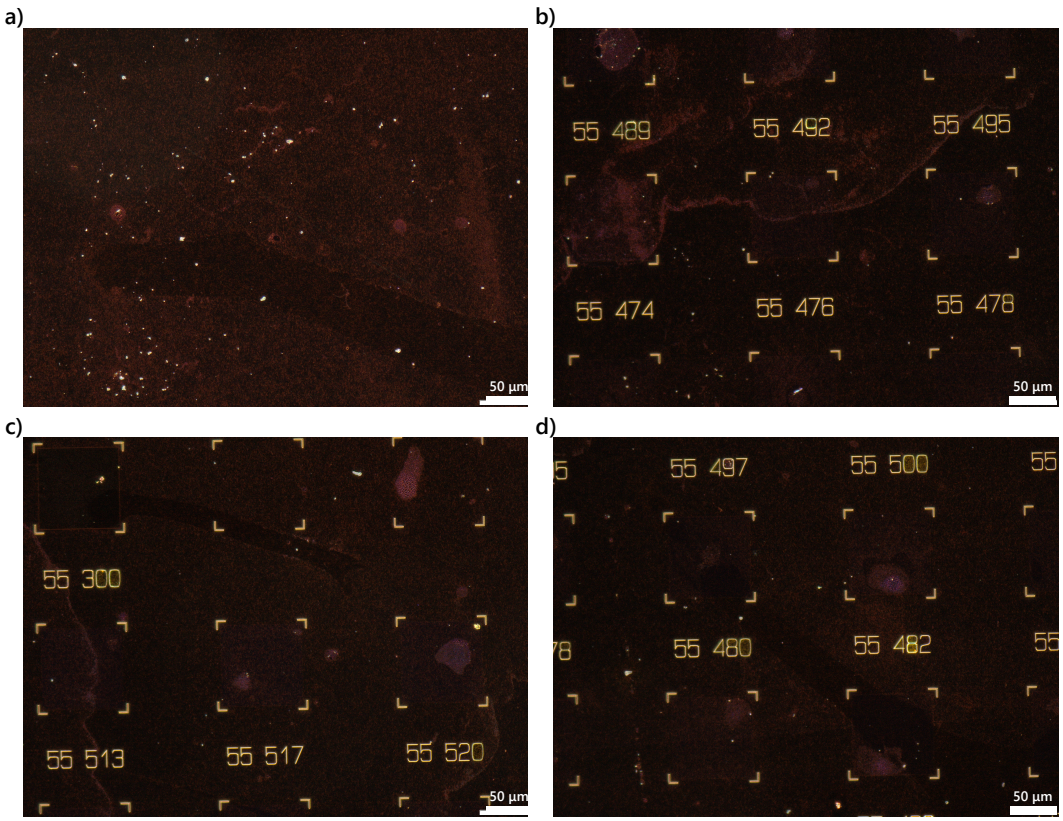

Figure A.1: a)-d) Dark-field microscope images at different positions on the sample.

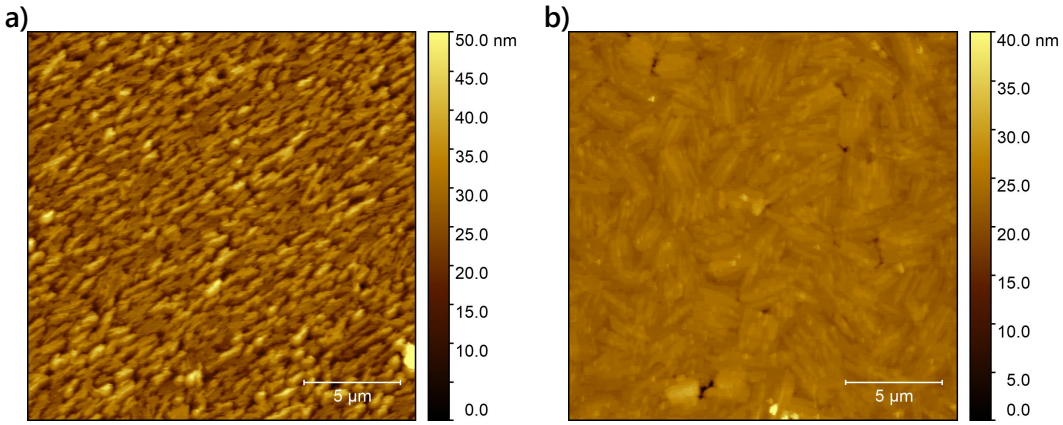

Figure A.2: Atomic force micrographs at two different positions next to a plasmonic lattice in the region, where molecular alignment is expected. Panel a) and b) show aligned and not aligned HB238 aggregates, respectively. Atomic force micrographs were measured and analyzed by Manuel Neubauer (working group of Prof. Meerholz).

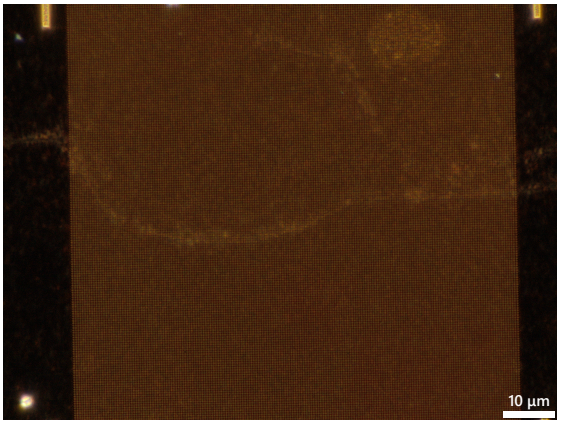

Figure A.3: Dark-field microscope image of a plasmonic nano-particle lattice with a period of 476 nm.

References

[1] V. Podzorov, "Organic single crystals: Addressing the fundamentals of organic electronics", *MRS Bulletin* **2013**, *38*, 15–24.

[2] C. W. Lee, O. Y. Kim, J. Y. Lee, "Organic materials for organic electronic devices", *Journal of Industrial and Engineering Chemistry* **2014**, *20*, 1198–1208.

[3] A. Köhler, *Electronic processes in organic semiconductors, An introduction*, (Ed.: H. Bässler), Wiley-VCH Verlag GmbH Co KGaA, Weinheim, **2015**.

[4] H. Sirringhaus, "25th Anniversary Article: Organic Field-Effect Transistors: The Path Beyond Amorphous Silicon", *Advanced Materials* **2014**, *26*, 1319–1335.

[5] Z. Hu, J. Wang, X. Ma, J. Gao, C. Xu, K. Yang, Z. Wang, J. Zhang, F. Zhang, "A critical review on semitransparent organic solar cells", *Nano Energy* **2020**, *78*, 105376.

[6] J. Song, H. Lee, E. G. Jeong, K. C. Choi, S. Yoo, "Organic Light-Emitting Diodes: Pushing Toward the Limits and Beyond", *Advanced Materials* **2020**, *32*, 1907539.

[7] C. R. Newman, R. J. Chesterfield, J. A. Merlo, C. D. Frisbie, "Transport properties of single–crystal tetracene field–effect transistors with silicon dioxide gate dielectric", *Applied Physics Letters* **2004**, *85*, 422–424.

[8] J. Takeya, T. Nishikawa, T. Takenobu, S. Kobayashi, Y. Iwasa, T. Mitani, C. Goldmann, C. Krellner, B. Batlogg, "Effects of polarized organosilane self–assembled monolayers on organic single–crystal field–effect transistors", *Applied Physics Letters* **2004**, *85*, 5078–5080.

[9] H. Zhao, Z. Wang, G. Dong, L. Duan, "Fabrication of highly oriented large–scale TIPS pentacene crystals and transistors by the Marangoni effect–controlled growth method", *Physical Chemistry Chemical Physics* **2015**, *17*, 6274–6279.

[10] F. Zhang, E. Mohammadi, X. Luo, J. Strzalka, J. Mei, Y. Diao, "Critical Role of Surface Energy in Guiding Crystallization of Solution–Coated Conjugated Polymer Thin Films", *Langmuir* **2017**, *34*, 1109–1122.

[11] C. Lee, T. Schiros, E. J. G. Santos, B. Kim, K. G. Yager, S. J. Kang, S. Lee, J. Yu, K. Watanabe, T. Taniguchi, J. Hone, E. Kaxiras, C. Nuckolls, P. Kim, "Epitaxial Growth of Molecular Crystals on van der Waals Substrates for High-Performance Organic Electronics", *Advanced Materials* **2014**, *26*, 2812–2817.

[12] F. J. Garcia-Vidal, C. Ciuti, T. W. Ebbesen, "Manipulating matter by strong coupling to vacuum fields", *Science* **2021**, *373*, eabd0336.

[13] D. G. Lidzey, D. D. C. Bradley, M. S. Skolnick, T. Virgili, S. Walker, D. M. Whittaker, “Strong exciton–photon coupling in an organic semiconductor microcavity”, *Nature* **1998**, *395*, 53–55.

[14] D. G. Lidzey, D. D. C. Bradley, T. Virgili, A. Armitage, M. S. Skolnick, S. Walker, “Room Temperature Polariton Emission from Strongly Coupled Organic Semiconductor Microcavities”, *Physical Review Letters* **1999**, *82*, 3316–3319.

[15] D. Timmer, M. Gittinger, T. Quenzel, S. Stephan, Y. Zhang, M. F. Schumacher, A. Lützen, M. Silies, S. Tretiak, J.-H. Zhong, A. De Sio, C. Lienau, “Plasmon mediated coherent population oscillations in molecular aggregates”, *Nature Communications* **2023**, *14*, 8035.

[16] S. Kéna-Cohen, S. R. Forrest, “Room–temperature polariton lasing in an organic single–crystal microcavity”, *Nature Photonics* **2010**, *4*, 371–375.

[17] A. I. Väkeväinen, R. J. Moerland, H. T. Rekola, A.-P. Eskelinen, J.-P. Martikainen, D.-H. Kim, P. Törmä, “Plasmonic Surface Lattice Resonances at the Strong Coupling Regime”, *Nano Letters* **2013**, *14*, 1721–1727.

[18] K. Srinivasan, P. E. Barclay, O. Painter, J. Chen, A. Y. Cho, C. Gmachl, “Experimental demonstration of a high quality factor photonic crystal microcavity”, *Applied Physics Letters* **2003**, *83*, 1915–1917.

[19] J. Gérard, B. Sermage, B. Gayral, B. Legrand, E. Costard, V. Thierry-Mieg, “Enhanced Spontaneous Emission by Quantum Boxes in a Monolithic Optical Microcavity”, *Physical Review Letters* **1998**, *81*, 1110–1113.

[20] B. Gayral, J. M. Gérard, A. Lematre, C. Dupuis, L. Manin, J. L. Pelouard, “High–Q wet–etched GaAs microdisks containing InAs quantum boxes”, *Applied Physics Letters* **1999**, *75*, 1908–1910.

[21] C. Schneider, A. Rahimi-Iman, N. Y. Kim, J. Fischer, I. G. Savenko, M. Amthor, M. Lermer, A. Wolf, L. Worschech, V. D. Kulakovskii, I. A. Shelykh, M. Kamp, S. Reitzenstein, A. Forchel, Y. Yamamoto, S. Höfling, “An electrically pumped polariton laser”, *Nature* **2013**, *497*, 348–352.

[22] A. Mischok, S. Hillebrandt, S. Kwon, M. C. Gather, “Highly efficient polaritonic light–emitting diodes with angle–independent narrowband emission”, *Nature Photonics* **2023**, *17*, 393–400.

[23] J. Q. Quach, K. E. McGhee, L. Ganzer, D. M. Rouse, B. W. Lovett, E. M. Gauger, J. Keeling, G. Cerullo, D. G. Lidzey, T. Virgili, “Superabsorption in an organic microcavity: Toward a quantum battery”, *Science Advances* **2022**, *8*, eabk3160.

[24] D. A. Sannikov, A. V. Baranikov, A. D. Putintsev, M. Misko, A. V. Zasedatelev, U. Scherf, P. G. Lagoudakis, "Room temperature, cascadable, all–optical polariton universal gates", *Nature Communications* **2024**, *15*, 5362.

[25] F. Le Roux, A. Mischok, D. D. C. Bradley, M. C. Gather, "Efficient Anisotropic Polariton Lasing Using Molecular Conformation and Orientation in Organic Microcavities", *Advanced Functional Materials* **2022**, *32*, 2209241.

[26] M. Litinskaya, P. Reineker, "Loss of coherence of exciton polaritons in inhomogeneous organic microcavities", *Physical Review B* **2006**, *74*, 165320.

[27] V. M. Agranovich, M. Litinskaia, D. G. Lidzey, "Cavity polaritons in microcavities containing disordered organic semiconductors", *Physical Review B* **2003**, *67*, 085311.

[28] G. Engelhardt, J. Cao, "Unusual dynamical properties of disordered polaritons in microcavities", *Physical Review B* **2022**, *105*, 064205.

[29] F. C. Spano, "Optical microcavities enhance the exciton coherence length and eliminate vibronic coupling in J–aggregates", *The Journal of Chemical Physics* **2015**, *142*.

[30] A. M. Berghuis, V. Serpenti, M. Ramezani, S. Wang, J. Gómez Rivas, "Light-Matter Coupling Strength Controlled by the Orientation of Organic Crystals in Plasmonic Cavities", *The Journal of Physical Chemistry C* **2020**, *124*, 12030–12038.

[31] A. M. Berghuis, R. H. Tichauer, L. M. A. de Jong, I. Sokolovskii, P. Bai, M. Ramezani, S. Murai, G. Groenhof, J. Gómez Rivas, "Controlling Exciton Propagation in Organic Crystals through Strong Coupling to Plasmonic Nanoparticle Arrays", *ACS Photonics* **2022**, *9*, 2263–2272.

[32] N. J. Herrmann, M. Hertzog, A. Mischok, M. C. Gather, J. Zaumseil, "Polarization–Dependent Strong and Weak Light–Matter Coupling in Aligned Perylene Diimide Thin Films", *ACS Applied Optical Materials* **2024**, *2*, 1619–1628.

[33] A. George, T. Geraghty, Z. Kelsey, S. Mukherjee, G. Davidova, W. Kim, A. J. Musser, "Controlling the Manifold of Polariton States Through Molecular Disorder", *Advanced Optical Materials* **2024**, *12*, 2302387.

[34] H. Bürckstümmer, E. V. Tulyakova, M. Deppisch, M. R. Lenze, N. M. Kronenberg, M. Gsänger, M. Stolte, K. Meerholz, F. Würthner, "Efficient SolutionProcessed Bulk Heterojunction Solar Cells by Antiparallel Supramolecular Arrangement of Dipolar DonorAcceptor Dyes", *Angewandte Chemie International Edition* **2011**, *50*, 11628–11632.

[35] L. Böhner, *Optical, morphological, and electrical properties of merocyanine molecular aggregate thin films – a correlated study*, Ph.D. Dissertation, University of Cologne, Cologne, Germany, **2022**.

[36] L. Böhner, P. Weitkamp, T. Limböck, N. Gildemeister, D. Fazzi, M. Schiek, R. Bruker, D. Hertel, R. Schäfer, K. Lindfors, K. Meerholz, "Influencing optical and charge transport properties by controlling the molecular interactions of merocyanine thin films", *Organic Chemistry Frontiers* **2025**, *12*, 1086–1098.

[37] P. Weitkamp, *Uniaxial alignment of organic semiconductors by armchair graphene nanoribbon templating*, Ph.D. Dissertation, University of Cologne, Cologne, Germany, **2024**.

[38] M. Litinskaya, P. Reineker, V. M. Agranovich, "Exciton–polaritons in a crystalline anisotropic organic microcavity", *physica status solidi (a)* **2004**, *201*, 646–654.

[39] H. Zoubi, G. La Rocca, "Microscopic theory of anisotropic organic cavity exciton polaritons", *Physical Review B* **2005**, *71*, 235316.

[40] S Kéna-Cohen, M. Davanço, S. R. Forrest, "Strong Exciton–Photon Coupling in an Organic Single Crystal Microcavity", *Physical Review Letters* **2008**, *101*, 116401.

[41] R. Guo, T. K. Hakala, P. Törmä, "Geometry dependence of surface lattice resonances in plasmonic nanoparticle arrays", *Physical Review B* **2017**, *95*, 155423.

[42] B. E. A. Saleh, *Fundamentals of photonics*, Third edition., (Ed.: M. C. Teich), Wiley, Hoboken, NJ, **2019**.

[43] A. Jablonski, "Über den Mechanismus der Photolumineszenz von Farbstoffphosphoren", *Zeitschrift für Physik* **1935**, *94*, 38–46.

[44] G. N. Lewis, M. Kasha, "Phosphorescence and the Triplet State", *Journal of the American Chemical Society* **1944**, *66*, 2100–2116.

[45] E. Fermi, *Nuclear physics: a course given by Enrico Fermi at the University of Chicago*, University of Chicago press, **1950**, pp. 103–116.

[46] A. Einstein, *Zur quantentheorie der strahlung*, Verlag u. Druck Gebr. Leemann, **1916**, pp. 209–228.

[47] A. V. Kavokin, J. J. Baumberg, G. Malpuech, F. P. Laussy, *Microcavities*, Oxford University PressOxford, **2017**.

[48] E. M. Purcell, "Spontaneous Emission Probabilities at Radio Frequencies", *Physical Review* **1946**, *69*, 681.

[49] E. M. Purcell, H. C. Torrey, R. V. Pound, "Resonance Absorption by Nuclear Magnetic Moments in a Solid", *Physical Review* **1946**, *69*, 37–38.

[50] D. Kleppner, “Inhibited Spontaneous Emission”, *Physical Review Letters* **1981**, *47*, 233–236.

[51] E. Yablonovitch, “Inhibited Spontaneous Emission in Solid-State Physics and Electronics”, *Physical Review Letters* **1987**, *58*, 2059–2062.

[52] S. Haroche, D. Kleppner, “Cavity Quantum Electrodynamics”, *Physics Today* **1989**, *42*, 24–30.

[53] A. Kress, F. Hofbauer, N. Reinelt, M. Kaniber, H. J. Krenner, R. Meyer, G. Böhm, J. J. Finley, “Manipulation of the spontaneous emission dynamics of quantum dots in two–dimensional photonic crystals”, *Physical Review B* **2005**, *71*, 241304.

[54] Y. Hiroyuki, K. Ujihara, *Spontaneous Emission and Laser Oscillation in Microcavities*, CRC Press, **2020**.

[55] D. G. Lidzey, D. M. Coles in *Organic and Hybrid Photonic Crystals*, Springer International Publishing, **2015**, pp. 243–273.

[56] L. Novotny, *Principles of nano–optics*, Second edition, (Ed.: B. Hecht), Cambridge University Press, Cambridge, **2012**.

[57] J. Tignon, P. Voisin, C. Delalande, M. Voos, R. Houdré, U. Oesterle, R. P. Stanley, “From Fermis Golden Rule to the Vacuum Rabi Splitting: Magnetopolaritons in a Semiconductor Optical Microcavity”, *Physical Review Letters* **1995**, *74*, 3967–3970.

[58] S. R.-K. Rodriguez, “Classical and quantum distinctions between weak and strong coupling”, *European Journal of Physics* **2016**, *37*, 025802.

[59] E. Jaynes, F. Cummings, “Comparison of quantum and semiclassical radiation theories with application to the beam maser”, *Proceedings of the IEEE* **1963**, *51*, 89–109.

[60] H. J. Carmichael, “Quantum fluctuations in absorptive bistability without adiabatic elimination”, *Physical Review A* **1986**, *33*, 3262–3269.

[61] M. Fox, *Quantum optics, An introduction*, Oxford University Press, **2006**.

[62] P. Törmä, W. L. Barnes, “Strong coupling between surface plasmon polaritons and emitters: a review”, *Reports on Progress in Physics* **2014**, *78*, 013901.

[63] J. M. Fink, R. Bianchetti, M. Baur, M. Göppl, L. Steffen, S. Filipp, P. J. Leek, A. Blais, A. Wallraff, “Dressed Collective Qubit States and the Tavis–Cummings Model in Circuit QED”, *Physical Review Letters* **2009**, *103*, 083601.

[64] J. J. Hopfield, “Theory of the Contribution of Excitons to the Complex Dielectric Constant of Crystals”, *Physical Review* **1958**, *112*, 1555–1567.

[65] F. Wu, D. Finkelstein-Shapiro, M. Wang, I. Rosenkampff, A. Yartsev, T. Pascher, T. C. Nguyen-Phan, R. Cogdell, K. Börjesson, T. Pullerits, "Optical cavity–mediated exciton dynamics in photosynthetic light harvesting 2 complexes", *Nature Communications* **2022**, *13*, 6864.

[66] M. S. Skolnick, T. A. Fisher, D. M. Whittaker, "Strong coupling phenomena in quantum microcavity structures", *Semiconductor Science and Technology* **1998**, *13*, 645–669.

[67] M. S. Rider, W. L. Barnes, "Something from nothing: linking molecules with virtual light", *Contemporary Physics* **2021**, *62*, 217–232.

[68] M. G. Raizen, R. J. Thompson, R. J. Brecha, H. J. Kimble, H. J. Carmichael, "Normal–mode splitting and linewidth averaging for two–state atoms in an optical cavity", *Physical Review Letters* **1989**, *63*, 240–243.

[69] C. Weisbuch, M. Nishioka, A. Ishikawa, Y. Arakawa, "Observation of the coupled exciton–photon mode splitting in a semiconductor quantum microcavity", *Physical Review Letters* **1992**, *69*, 3314–3317.

[70] J. P. Reithmaier, G. Sk, A. Löffler, C. Hofmann, S. Kuhn, S. Reitzenstein, L. V. Keldysh, V. D. Kulakovskii, T. L. Reinecke, A. Forchel, "Strong coupling in a single quantum dotsemiconductor microcavity system", *Nature* **2004**, *432*, 197–200.

[71] J. A. Hutchison, T. Schwartz, C. Genet, E. Devaux, T. W. Ebbesen, "Modifying Chemical Landscapes by Coupling to Vacuum Fields", *Angewandte Chemie International Edition* **2012**, *51*, 1592–1596.

[72] A. Thomas, J. George, A. Shalabney, M. Dryzhakov, S. J. Varma, J. Moran, T. Chervy, X. Zhong, E. Devaux, C. Genet, J. A. Hutchison, T. W. Ebbesen, "Ground-State Chemical Reactivity under Vibrational Coupling to the Vacuum Electromagnetic Field", *Angewandte Chemie International Edition* **2016**, *55*, 11462–11466.

[73] J. Dutta, N. Yadav, P. Bhatt, K. Kaur, D. E. Gómez, J. George, "Enhanced Energy Transfer in Cavity QED Based Phototransistors", *The Journal of Physical Chemistry Letters* **2024**, *15*, 8211–8217.

[74] P. Bhatt, K. Kaur, J. George, "Enhanced Charge Transport in Two–Dimensional Materials through LightMatter Strong Coupling", *ACS Nano* **2021**, *15*, 13616–13622.

[75] E. Orgiu, J. George, J. A. Hutchison, E. Devaux, J. F. Dayen, B. Doudin, F. Stellacci, C. Genet, J. Schachenmayer, C. Genes, G. Pupillo, P. Samorì, T. W. Ebbesen, "Conductivity in organic semiconductors hybridized with the vacuum field", *Nature Materials* **2015**, *14*, 1123–1129.

[76] R. Pandya, R. Y. S. Chen, Q. Gu, J. Sung, C. Schnedermann, O. S. Ojambati, R. Chikkaraddy, J. Gorman, G. Jacucci, O. D. Onelli, T. Willhammar, D. N. Johnstone, S. M. Collins, P. A. Midgley, F. Auras, T. Baikie, R. Jayaprakash, F. Mathevet, R. Soucek, M. Du, A. M. Alvertis, A. Ashoka, S. Vignolini, D. G. Lidzey, J. J. Baumberg, R. H. Friend, T. Barisien, L. Legrand, A. W. Chin, J. Yuen-Zhou, S. K. Saikin, P. Kukura, A. J. Musser, A. Rao, "Microcavity–like exciton–polaritons can be the primary photoexcitation in bare organic semiconductors", *Nature Communications* **2021**, *12*, 6519.

[77] R. K. Yadav, M. Otten, W. Wang, C. L. Cortes, D. J. Gosztola, G. P. Wiederrecht, S. K. Gray, T. W. Odom, J. K. Basu, "Strongly Coupled ExcitonSurface Lattice Resonances Engineer Long–Range Energy Propagation", *Nano Letters* **2020**, *20*, 5043–5049.

[78] D. M. Coles, N. Somaschi, P. Michetti, C. Clark, P. G. Lagoudakis, P. G. Savvidis, D. G. Lidzey, "Polariton–mediated energy transfer between organic dyes in a strongly coupled optical microcavity", *Nature Materials* **2014**, *13*, 712–719.

[79] K. Georgiou, P. Michetti, L. Gai, M. Cavazzini, Z. Shen, D. G. Lidzey, "Control over Energy Transfer between Fluorescent BODIPY Dyes in a Strongly Coupled Microcavity", *ACS Photonics* **2017**, *5*, 258–266.

[80] K. S. Daskalakis, S. A. Maier, R. Murray, S. Kéna-Cohen, "Nonlinear interactions in an organic polariton condensate", *Nature Materials* **2014**, *13*, 271–278.

[81] H. Becker, S. E. Burns, N. Tessler, R. H. Friend, "Role of optical properties of metallic mirrors in microcavity structures", *Journal of Applied Physics* **1997**, *81*, 2825–2829.

[82] E. Hecht, *Optik*, De Gruyter, **2023**.

[83] S. A. Maier, *Plasmonics: Fundamentals and Applications*, Springer US, **2007**.

[84] A. Derkachova, K. Kolwas, I. Demchenko, "Dielectric Function for Gold in Plasmonics Applications: Size Dependence of Plasmon Resonance Frequencies and Damping Rates for Nanospheres", *Plasmonics* **2015**, *11*, 941–951.

[85] G. L. Eesley, "Generation of nonequilibrium electron and lattice temperatures in copper by picosecond laser pulses", *Physical Review B* **1986**, *33*, 2144–2151.

[86] M. Agio, "Optical antennas as nanoscale resonators", *Nanoscale* **2012**, *4*, 692–706.

[87] V. G. Kravets, A. V. Kabashin, W. L. Barnes, A. N. Grigorenko, "Plasmonic Surface Lattice Resonances: A Review of Properties and Applications", *Chemical Reviews* **2018**, *118*, 5912–5951.

[88] N. Maccaferri, G. Barbillon, A. N. Koya, G. Lu, G. P. Acuna, D. Garoli, "Recent advances in plasmonic nanocavities for single–molecule spectroscopy", *Nanoscale Advances* **2021**, *3*, 633–642.

[89] S. Link, M. A. El-Sayed, "Shape and size dependence of radiative, non–radiative and photothermal properties of gold nanocrystals", *International Reviews in Physical Chemistry* **2000**, *19*, 409–453.

[90] G. Zengin, G. Johansson, P. Johansson, T. J. Antosiewicz, M. Käll, T. Shegai, "Approaching the strong coupling limit in single plasmonic nanorods interacting with J–aggregates", *Scientific Reports* **2013**, *3*, 3074.

[91] B. Auguié, W. L. Barnes, "Collective Resonances in Gold Nanoparticle Arrays", *Physical Review Letters* **2008**, *101*, 143902.

[92] V. G. Kravets, F. Schedin, A. N. Grigorenko, "Extremely Narrow Plasmon Resonances Based on Diffraction Coupling of Localized Plasmons in Arrays of Metallic Nanoparticles", *Physical Review Letters* **2008**, *101*, 087403.

[93] S. Rodriguez, M. Schaafsma, A. Berrier, J. Gómez Rivas, "Collective resonances in plasmonic crystals: Size matters", *Physica B: Condensed Matter* **2012**, *407*, 4081–4085.

[94] F. Würthner, T. E. Kaiser, C. R. SahaMöller, "JAggregates: From Serendipitous Discovery to Supramolecular Engineering of Functional Dye Materials", *Angewandte Chemie International Edition* **2011**, *50*, 3376–3410.

[95] N. J. Hestand, F. C. Spano, "Expanded Theory of H– and J–Molecular Aggregates: The Effects of Vibronic Coupling and Intermolecular Charge Transfer", *Chemical Reviews* **2018**, *118*, 7069–7163.

[96] E. E. Jelley, "Spectral Absorption and Fluorescence of Dyes in the Molecular State", *Nature* **1936**, *138*, 1009–1010.

[97] G. Scheibe, L. Kandler, H. Ecker, "Polymerisation und polymere Adsorption als Ursache neuartiger Absorptionsbanden von organischen Farbstoffen", *Die Naturwissenschaften* **1937**, *25*, 75–75.

[98] G. Scheibe, "Über die Veränderlichkeit der Absorptionsspektren in Lösungen und die Nebenvalenzen als ihre Ursache", *Angewandte Chemie* **1937**, *50*, 212–219.

[99] H. von Berlepsch, C. Böttcher, L. Dähne, "Structure of J–Aggregates of Pseudoisocyanine Dye in Aqueous Solution", *The Journal of Physical Chemistry B* **2000**, *104*, 8792–8799.

[100] B. Herzog, K. Huber, H. Stegemeyer, "Aggregation of a Pseudoisocyanine Chloride in Aqueous NaCl Solution", *Langmuir* **2003**, *19*, 5223–5232.

[101] S. Liu, W. M. Wang, A. L. Briseno, S. C. B. Mannsfeld, Z. Bao, "Controlled Deposition of Crystalline Organic Semiconductors for FieldEffectTransistor Applications", *Advanced Materials* **2009**, *21*, 1217–1232.

[102] F. C. Spano, "Analysis of the UV/Vis and CD Spectral Line Shapes of Carotenoid Assemblies: Spectral Signatures of Chiral H–Aggregates", *Journal of the American Chemical Society* **2009**, *131*, 4267–4278.

[103] U. Rösch, S. Yao, R. Wortmann, F. Würthner, "Fluorescent HAggregates of Merocyanine Dyes", *Angewandte Chemie* **2006**, *118*, 7184–7188.

[104] A. Eisfeld, J. Briggs, "The J– and H–bands of organic dye aggregates", *Chemical Physics* **2006**, *324*, 376–384.

[105] M. Kasha, "Energy Transfer Mechanisms and the Molecular Exciton Model for Molecular Aggregates", *Radiation Research* **1963**, *20*, 55.

[106] M. Kasha, H. R. Rawls, M. Ashraf El-Bayoumi, "The exciton model in molecular spectroscopy", *Pure and Applied Chemistry* **1965**, *11*, 371–392.

[107] M. Kasha, "Characterization of electronic transitions in complex molecules", *Discussions of the Faraday Society* **1950**, *9*, 14.

[108] I. Scheblykin, M. Bataiev, M. Van der Auweraer, A. Vitukhnovsky, "Dimensionality and temperature dependence of the radiative lifetime of J–aggregates with Davydov splitting of the exciton band", *Chemical Physics Letters* **2000**, *316*, 37–44.

[109] A. S. Davydov, "The theory of molecular excitons", *Soviet Physics Uspekhi* **1964**, *7*, 145–178.

[110] A. S. Davydov, *Theory of Molecular Excitons*, Springer US, Boston, MA, **1971**.

[111] A. Jumbo-Nogales, V. Krivenkov, K. Rusakov, A. S. Urban, M. Grzelczak, Y. P. Rakovich, "Cross Determination of Exciton Coherence Length in J–Aggregates", *The Journal of Physical Chemistry Letters* **2022**, *13*, 10198–10206.

[112] R. Schäfer, L. Böhner, M. Schiek, D. Hertel, K. Meerholz, K. Lindfors, "Strong Light–Matter Interaction of Molecular Aggregates with Two Excitonic Transitions", *ACS Photonics* **2023**, *11*, 111–120.

[113] A. Liess, A. Lv, A. Arjona-Esteban, D. Bialas, A.-M. Krause, V. Stepanenko, M. Stolte, F. Würthner, "Exciton Coupling of Merocyanine Dyes from H– to J–type in the Solid State by Crystal Engineering", *Nano Letters* **2017**, *17*, 1719–1726.

[114] A. Liess, A. Arjona-Esteban, A. Kudzus, J. Albert, A. Krause, A. Lv, M. Stolte, K. Meerholz, F. Würthner, "Ultranarrow Bandwidth Organic Photodiodes by Exchange Narrowing in Merocyanine H and JAggregate Excitonic Systems", *Advanced Functional Materials* **2019**, *29*, 1805058.

[115] A. B. Vasista, D. K. Sharma, G. P. Kumar, "Fourier Plane Optical Microscopy and Spectroscopy", *digital Encyclopedia of Applied Physics* **2019**, 1–14.

[116] M. A. Lieb, J. M. Zavislan, L. Novotny, "Single–molecule orientations determined by direct emission pattern imaging", *Journal of the Optical Society of America B* **2004**, *21*, 1210.

[117] I. Sersic, C. Tuambilangana, A. F. Koenderink, "Fourier microscopy of single plasmonic scatterers", *New Journal of Physics* **2011**, *13*, 083019.

[118] R. Wagner, L. Heerklotz, N. Kortenbruck, F. Cichos, "Back focal plane imaging spectroscopy of photonic crystals", *Applied Physics Letters* **2012**, *101*, 081904.

[119] Y. Zhang, M. Zhao, J. Wang, W. Liu, B. Wang, S. Hu, G. Lu, A. Chen, J. Cui, W. Zhang, C. W. Hsu, X. Liu, L. Shi, H. Yin, J. Zi, "Momentum–space imaging spectroscopy for the study of nanophotonic materials", *Science Bulletin* **2021**, *66*, 824–838.

[120] Thorlabs, Diffraction Gratings Tutorial, `https://www.thorlabs.com/newgrouppage9.cfm?objectgroup_id=9026`, Accessed: 24.03.2025.

[121] M. Ovesný, P. Kíek, J. Borkovec, Z. vindrych, G. M. Hagen, "ThunderSTORM: a comprehensive ImageJ plug–in for PALM and STORM data analysis and super–resolution imaging", *Bioinformatics* **2014**, *30*, 2389–2390.

[122] M. Born, *Principles of optics*, Seventh anniversary edition, (Eds.: E. Wolf, A. B. Bhatia, P. Knight), Cambridge University Press, Cambridge, **2019**.

[123] M. J. Rust, M. Bates, X. Zhuang, "Sub–diffraction–limit imaging by stochastic optical reconstruction microscopy (STORM)", *Nature Methods* **2006**, *3*, 793–796.

[124] D. W. Pohl, U. C. Fischer, U. T. Dürig, "Scanning nearfield optical microscopy (SNOM)", *Journal of Microscopy* **1988**, *152*, 853–861.

[125] H. Heinzelmann, D. W. Pohl, "Scanning near–field optical microscopy", *Applied Physics A Solids and Surfaces* **1994**, *59*, 89–101.

[126] R. R. Gutha, S. M. Sadeghi, C. Sharp, W. J. Wing, "Biological sensing using hybridization phase of plasmonic resonances with photonic lattice modes in arrays of gold nanoantennas", *Nanotechnology* **2017**, *28*, 355504.

[127] W. Zhou, M. Dridi, J. Y. Suh, C. H. Kim, D. T. Co, M. R. Wasielewski, G. C. Schatz, T. W. Odom, "Lasing action in strongly coupled plasmonic nanocavity arrays", *Nature Nanotechnology* **2013**, *8*, 506–511.

[128] A. Yang, T. B. Hoang, M. Dridi, C. Deeb, M. H. Mikkelsen, G. C. Schatz, T. W. Odom, "Real–time tunable lasing from plasmonic nanocavity arrays", *Nature Communications* **2015**, *6*, 6939.

[129] D. Wang, A. Yang, W. Wang, Y. Hua, R. D. Schaller, G. C. Schatz, T. W. Odom, "Band–edge engineering for controlled multi–modal nanolasing in plasmonic superlattices", *Nature Nanotechnology* **2017**, *12*, 889–894.

[130] R. Tomar, L. Bernasconi, D. Fazzi, T. Bredow, "Theoretical Study on the Optoelectronic Properties of Merocyanine–Dyes", *The Journal of Physical Chemistry A* **2023**, *127*, 9661–9671.

[131] N. Gildemeister, G. Ricci, L. Böhner, J. M. Neudörfl, D. Hertel, F. Würthner, F. Negri, K. Meerholz, D. Fazzi, "Understanding the structural and charge transport property relationships for a variety of merocyanine single–crystals: a bottom up computational investigation", *Journal of Materials Chemistry C* **2021**, *9*, 10851–10864.

[132] R. Schäfer, P. Weitkamp, O. Erdene-Ochir, K. Meerholz, K. Lindfors, "Polarization–controlled strong light–matter interaction with templated molecular aggregates", *arXiv preprint* **2025**, arXiv:2503.09798.

[133] B. Öcal, P. Weitkamp, K. Meerholz, S. Olthof, "Chemical interaction and molecular growth of a highly dipolar merocyanine molecule on metal surfaces: A photoelectron spectroscopy study", *Surface Science* **2025**, *754*, 122690.

[134] A. J. Kny, M. Reimer, N. Al-Shamery, R. Tomar, T. Bredow, S. Olthof, D. Hertel, K. Meerholz, M. Sokolowski, "Chiral self–organized single 2D-layers of tetramers from a functional donor-acceptor molecule by the surface template effect", *Nanoscale* **2023**, *15*, 10319–10329.

[135] D. Wang, A. Yang, A. J. Hryn, G. C. Schatz, T. W. Odom, "Superlattice Plasmons in Hierarchical Au Nanoparticle Arrays", *ACS Photonics* **2015**, *2*, 1789–1794.

[136] S. Rodriguez, J. G. Rivas, "Surface lattice resonances strongly coupled to Rhodamine 6G excitons: tuning the plasmon–exciton–polariton mass and composition", *Optics Express* **2013**, *21*, 27411.

[137] J. Sun, S. Deng, W. Guo, Z. Zhan, J. Deng, C. Xu, X. Fan, K. Xu, W. Guo, Y. Huang, X. Liu, "Electrochemical Bubbling Transfer of Graphene Using a Polymer Support with Encapsulated Air Gap as Permeation Stopping Layer", *Journal of Nanomaterials* **2016**, *2016*, 1–7.

[138] D. Neas, P. Klapetek, "Gwyddion: an open–source software for SPM data analysis", *Central European Journal of Physics* **2012**, *10*, 181–188.

[139] P. B. Johnson, R. W. Christy, "Optical Constants of the Noble Metals", *Physical Review B* **1972**, *6*, 4370–4379.

Personal bibliography

Publications

R. Schäfer, L. Böhner, M. Schiek, D. Hertel, K. Meerholz, and K. Lindfors, *ACS Photonics* **2023**, *11*, 111–120.
DOI: https://doi.org/10.1021/acsphotonics.3c01042

R. Schäfer, P. Weitkamp, O. Erdene-Ochir, K. Meerholz, and K. Lindfors, *arXiv preprint arXiv:2503.09798* **2025**.
DOI: https://doi.org/10.48550/arXiv.2503.09798
Under revision at the journal of Advanced Optical Materials.

L. Böhner, P. Weitkamp, T. Limböck, N. Gildemeister, D. Fazzi, M. Schiek, R. Bruker, D. Hertel, **R. Schäfer**, K. Lindfors, and K. Meerholz, *Organic Chemistry Frontiers*, **2025**, *12*, 1086-1098.
DOI: https://doi.org/10.1039/d4qo02088j

R. Schäfer, M. Neubauer, K. Meerholz, and K. Lindfors, *arXiv preprint arXiv:2505.17983* **2025**.
DOI: https://doi.org/10.48550/arXiv.2505.17983

Conference Contributions - Talks

R. Schäfer, L. Böhner, M. Schiek, K. Meerholz, K. Lindofors "Simultaneous strong coupling of the H- and J-bands of molecular aggregates in microcavities", *DPG Spring Meeting of the Condensed Matter Section* **2023**, Dresden, Germany.

R. Schäfer, P. Weitkamp, D. Hertel, K. Meerholz, K. Lindfors "Polarization-controlled strong light-matter interaction with templated molecular aggregates", *1st TIDE International Research Conference* **2024**, Cologne, Germany.

R. Schäfer, P. Weitkamp, D. Hertel, K. Meerholz, K. Lindfors "Highly polarization dependent formation of polaritons due to molecular alignment", *DPG Spring Meeting of the Condensed Matter Section* **2024**, Berlin, Germany.

R. Schäfer, P. Weitkamp, O. Erdene-Ochir, D. Hertel, K. Meerholz, and K. Lindfors[1] "Probing the order of uniaxially aligned molecular aggregates via strong-light matter interaction", *17th International Conference on Near-field Optics, Nanophotonics, and Related Techniques (NFO-17)* **2024**, Melbourne, Australia.

[1] Due to personal reasons the talk was presented by K. Lindfors.

Conference Contributions - Poster

R. Schäfer, L. Bohner, M. Schiek, D. Hertel, K. Meerholz, K. Lindfors, "Simultaneous strong light–matter coupling of the H- and J-like excitonic transitions of a molecular aggregate", *Optical Probes* **2023**, Como, Italy.

List of abbreviations

AOI angle of incidence

CQED cavity quantum electrodynamics

DO diffraction order

7-AGNRs seven-atom wide armchair-edge graphene nanoribbons

LSPR localized surface plasmon resonances

NA numerical aperture

PL photoluminescence

QED quantum electrodynamics

SLR surface lattice resonances

TDM transition dipole moment